Detection of Ship Plumes from Residual Fuel Operation in Emission Control Areas using Single-Particle Mass Spectrometry

Johannes Passig[1,2,3], Julian Schade[2,3], Robert Irsig[3,4], Lei Li[5,6], Xue Li[5,6], Zhen Zhou[5,6], Thomas Adam[1,7] and Ralf Zimmermann[1,2,3]

[1]Joint Mass Spectrometry Centre, Helmholtz Zentrum München, 85764 Neuherberg, Germany
[2]Joint Mass Spectrometry Centre, Analytical Chemistry, University Rostock, 18059 Rostock, Germany
[3]Department Life, Light & Matter, University of Rostock, 18051 Rostock, Germany
[4]Photonion GmbH, 19061 Schwerin, Germany
[5]Institute of Mass Spectrometry and Atmospheric Environment, Jinan University, Guangzhou 510632, China
[6]Guangzhou Hexin Instrument Co., Ltd, Guangzhou 510530, China
[7]Universität der Bundeswehr München, 85577 Neubiberg, Germany

Correspondence to: Johannes Passig (johannes.passig@uni-rostock.de)

Abstract. Ships are main contributors to global air pollution with substantial impacts on climate and public health. To improve air quality in densely populated coastal areas and to protect sensitive ecosystems, sulfur emission control areas (SECA) were established in many regions of the world. Ships in SECAs operate with low-sulfur fuels, typically distillate fractions such as marine gas oil (MGO). Alternatively, exhaust gas cleaning devices ('scrubbers') can be implemented to remove SO_2 from the exhaust, thus allowing the use of cheap high-sulfur residual fuels. Compliance monitoring is established in harbors, but difficult in open water because of high costs and technical limitations. Here we present the first experiments to detect individual ship plumes from distances of several kilometers by single-particle mass spectrometry (SPMS). In contrast to most monitoring approaches that evaluate the gaseous emissions, such as manned or unmanned surveillance flights, sniffer technologies and remote sensing, we analyze the ~~chemical composition~~metal content of ~~the particulate phase~~ individual particles ~~that~~ which is ~~transported~~ conserved during atmospheric transport~~by the wind over long distances~~. We optimized SPMS technology for the evaluation of residual fuel emissions and demonstrate their detection in a SECA. Our experiments show that ships with installed scrubbers can emit PM emissions with health-relevant metals in quantities high enough to be detected from more than 10 km distance, emphasizing the importance of novel exhaust cleaning technologies and cleaner fuels. Because of the unique and stable ~~metal~~ signatures, the~~ir~~ method is not affected by urban background. With this study, we establish a route towards a novel monitoring protocol for ship emissions. Therefore, we present and discuss mass spectral signatures that indicate the particle age, and thus the distance to the source. By matching ship transponder data, measured wind data and air mass back trajectories, we show, how real-time SPMS data can be evaluated to assign distant ship passages.

1 Introduction

Among the variety of air pollution sources, ships emit particular large amounts of sulfur, carbonaceous aerosols and metals with substantial impacts on climate and public health (Corbett et al., 2007; Eyring et al., 2010; Viana et al., 2014; Jonson et al., 2020). Between 60,000 and 400,000 annual deaths by cardiopulmonary diseases and lung cancer as well as 14 million cases of childhood asthma were attributed to ship emissions (Sofiev et al., 2018). Mitigation strategies focus on the sulfur aspect, e.g. by a global 0.5% standard for ship fuels since 2020 and by implementation of Sulfur Emission Control Areas (SECA, <0.1% S in fuel mass since 2015) that currently comprise the Baltic Sea, the North Sea, and most of the U.S. and Canadian coast. Legal alternatives to the use of expensive distillate fuels in SECAs include desulfurized 'hybrid' blends of low-grade residual fuels (Lähteenmäki-Uutela et al., 2019) or the installation of exhaust cleaning devices for SO_2 like flue gas scrubbers (Winnes et al., 2018; Lehtoranta et al., 2019; Winnes et al., 2020).

Several studies investigated the effect of fuel composition on ship emissions and their respective effects on climate (Lack et al., 2011; Sofiev et al., 2018; Yu et al., 2020; Corbin et al., 2019) and health (Winebrake et al., 2009; Oeder et al., 2015). Beyond the SO_2 emissions, also the particle-phase pollution is specifically serious if low-grade heavy fuel oils (bunker fuels) are used (Moldanová et al., 2009; Sippula et al., 2014; Streibel et al., 2017; Di Wu et al., 2018). Within the various health effects of such combustion particles, specific risks for acute cardiovascular effects were associated with water-soluble fractions of particle-bound metals (Ye et al., 2018). Of note, iron solubility is promoted by the presence of sulfur (Fang et al., 2017), a situation that particularly arises for ship emission particles. Implementation of the sulfur regulations substantially decreased the use of residual fuels in SECAs (Jonson et al., 2019; Lähteenmäki-Uutela et al., 2019). However, ~~of~~ scrubber operation and combustion of desulfurized residual fuels reduce PM emissions only partially (Fridell and Salo, 2016; Lehtoranta et al., 2019; Winnes et al., 2020) and there is vital interest to assess the environmental and health effects (Winnes et al., 2018). Furthermore, compliance monitoring and emission inventories would benefit from the ability to distinguish between these options for ship operation.

Compliance monitoring on short distances is typically based on gas phase measurements of CO_2 and SO_2 in the plume of passing ships in harbors or at bridges (Kattner et al., 2015; Mellqvist et al., 2017b; Zhang et al., 2019). However, these places are known to be monitored, and also on-board checks occur frequently (Lähteenmäki-Uutela et al., 2019). Plume analyses in open water requires expensive surveillance flights (Beecken et al., 2014; Van Roy, W and Scheldemann, K., 2016). Unmanned aerial vehicles can reduce these costs but have limitations in cruising range, payload and weather conditions (Zhou et al., 2020). Optical sensing technologies that have been utilized to monitor ship plumes on few-km distances comprise light detection and ranging (LIDAR), ultraviolet cameras and multi-axis differential optical absorption spectroscopy (MAX-DOAS) (Balzani Lööv et al., 2014; Seyler et al., 2017).

~~Monitoring techniques based on gas phase measurements are limited in range because the gases rapidly mix with ambient air.~~ Particles often preserve source-specific chemical signatures ~~In contrast, particles~~ while being ~~are~~ transported by the wind over large~~ong~~ distances. Field studies on particulate matter (PM) from ship plumes can be performed by following ships at some

Feldfunktion geändert

hundred meters to few kilometers distance (Chen, 2005; Lack et al., 2009; Petzold et al., 2008; Berg et al., 2012). A different approach to characterize ship plumes are stationary ambient measurements downwind of shipping lanes while recording the ship transponder data (Automatic Identification System, AIS) (Diesch et al., 2013). Recently, Ausmeel et al. measured physical and chemical properties of more than 150 ship plumes in the Baltic Sea from a distance of about 10 km (Ausmeel et al., 2019; Ausmeel et al., 2020) and Celik et al. characterized 252 ship plumes in the Mediterranean Sea and around the Arabian Peninsula in distances up to 40 km from an ship-based measurement station (Celik et al., 2020). Such~~This~~ methods determine~~s~~ the presence of a ship plume mainly by an increase in particle number and changes in its size distribution or by an increase of a marker substance in the particle ensemble. Dispersion models of ship plumes showed rapid decrease in particle number concentration within the first minutes after emission (Tian et al., 2014; Celik et al., 2020). Therefore, particle number-based methods as well as particle integrating approaches are ~~restricted~~ limited to low background levels and ~~additional~~clear chemical indicators for ship plume presence combined with single-particle information may push the limits of stationary ambient measurements.

Established markers for aerosols from residual fuel combustion are combinations of vanadium, iron and nickel (Celo et al., 2015; Zhang et al., 2014). Single-particle mass spectrometry (SPMS) can detect these particle-bound metals in real time (Pratt and Prather, 2012; Passig and Zimmermann, 2021). ~~time~~ (Pratt and Prather, 2012; Zimmermann, Ralf and Hanley, Luke). Briefly, after optical sizing and introduction into vacuum, particles are exposed to intense UV laser pulses that form a microplasma (laser desorption/ionization, LDI). Both positive and negative ions are analyzed with respect to their mass-to-charge ratio (m/z). Thus, the size and a chemical profile from individual particles is obtained. SPMS studies documented air pollution by regional transport of emissions from harbors and shipping lanes (Reinard et al., 2007; Ault et al., 2009; Arndt et al., 2017; Gaston et al., 2013; Liu et al., 2017; Wang et al., 2019). Also individual ship plumes were analyzed by in-port studies (Healy et al., 2009; Ault et al., 2010; Xiao et al., 2018), demonstrating that SPMS can distinguish between residual fuel combustion and distillate fuel operation, predominantly by the metal signatures. All these studies were performed outside SECA zones, and, for the individual plume analyses, on short distances to the ships.

With the present study, we apply SPMS with resonant ionization of iron (Passig et al., 2020) for the detection of individual ship plumes from the distance to evaluate residual fuel combustion in SECA, also for ships equipped with scrubbers. We show that this approach is independent from background air pollution and we discuss the limits of detection over large distances. By examining indicators for particle ageing and the effects of inaccuracies in wind field determination, we pave the way to future open-sea monitoring of ship plumes using SPMS.

2 Experimental

2.1 Single-particle mass spectrometer and sampling

The SPMS was manufactured by Hexin Instruments Ltd., Guangzhou, China, and Photonion GmbH, Schwerin, Germany (Li et al., 2011; Zhou et al., 2016). It consists of a dual-polarity mass spectrometer in Z-TOF geometry (Pratt et al., 2009), an

Feldfunktion geändert

aerodynamic lens inlet and 75 mW continuous-wave lasers (wavelength λ=532 nm), ellipsoidal mirrors and photomultipliers for particle detection and sizing. The instrument is equipped with a KrF-excimer laser (λ=248.3 nm, PhotonEx, Photonion GmbH, Germany). The used wavelength is well-suited for resonance-enhanced laser desorption/ionization (LDI) of iron (Passig et al., 2020). Setting the lens (f=200 mm) to an off-focus position of 7 mm with respect to the particle beam, the spot size was about 150x300 µm and the resulting intensity 5 GW/cm^2 at 6 mJ pulse energy. The off-focus position in conjunction with the flat-top profile of the excimer laser beam allows hit rates around 50% (particles producing mass spectra vs. optically detected particles) (Schade et al., 2019; Passig et al., 2020).

The setup was housed in the southern periphery of the town Rostock (population 210,000) contributing urban background aerosols in between the sampling site and the coast. Possible regional aerosol sources comprise the urban area of Rostock, forests in north-eastern direction and farmland in the surrounding area, see Fig. 1.

Ambient air was sampled directly on the roof of the laboratory building (54°04'41.5"N 12°06'30.6"E), ~~at a height of~~ about 35 m above sea level. Because the study focuses on particles from distant sources, the sampling was optimized for larger particles ≳0.5 µm size at the expense of efficiency for smaller particles, such as local traffic emissions. Therefore, an aerosol concentrator, originally designed for particles above 2 µm size,~~–~~ was used (Model 4240, MSP corp., USA) (Romay et al., 2002). The multi-stage virtual impactor of this device concentrates particles from the 300 $L\,min^{-1}$ intake airflow into a 1 $L\,min^{-1}$ carrier gas stream, from which 0.1 $L\,min^{-1}$ were finally guided into the SPMS instrument. The real concentration factor for ambient air particles around 0.5 µm size was approximately 10:1, as estimated in previous experiments (Passig et al., 2020). Corrections of the inlet efficiency have not been applied.

Feldfunktion geändert

Feldfunktion geändert

Feldfunktion geändert

Feldfunktion geändert

2.2 Analysis of single-particle mass spectra

Using custom software on MATLAB platform (MathWorks Inc.), mass spectra were computed from time-of-flight data considering peak area within nominal mass resolution. Positive and negative mass spectra including the metal signatures were separately normalized and missing negative ion spectra were set to zero. We classified the particles using the adaptive resonance theory neural network, ART-2a (Song et al., 1999) extracted from the open-source toolkit FATES (Flexible Analysis Toolkit for the Exploration of SPMS data) (Sultana et al., 2017) with a learning rate 0.05, a vigilance factor of 0.8 and 20 iterations. ~~In short, positive and negative mass spectra of an individual particle are combined to one vector. Beginning with a randomly chosen spectrum, the inner products of every new spectrum with the weight vectors (already existing classes of particles) are calculated. The weight vector producing the highest inner product with the current particle is updated and the particle is assigned to this class, if the inner product exceeds the vigilance factor. Thus, the classes are iteratively adapted to the particle ensemble. If product is below this criterion, the current spectrum is considered as new weight vector (class).~~

Ion peak assignments corresponds to the most likely ion at a given mass (m/z). It should be noted, that SPMS obtains numbers of particles with particular chemical signatures, not the mass concentration of these components.

Feldfunktion geändert

Feldfunktion geändert

2.3 Meteorological and ship transponder data

~~The setup was housed in the southern periphery of the town Rostock (population 210,000) contributing urban background aerosols in between the sampling site and the coast. Possible regional aerosol sources comprise the urban area of Rostock, forests in north-eastern direction and farmland in the surrounding area, see Fig. 1.~~

Air trajectories were calculated using the interactive HYSPLIT web tool from the National Oceanic and Atmospheric Administration, model GDAS with 0.5° resolution (http://www.ready.noaa.gov/HYSPLIT.php, last access ~~10~~ 24 ~~November~~ March 202~~10~~) (Stein et al., 2015). Hourly wind data was obtained from the web archive of a local meteorological station that belongs to Germany's National Meteorological Service, 12 km north of the sampling site and close to the harbor exit (https://www.dwd.de/DE/leistungen/klimadatendeutschland/klarchivstunden.html#buehneTop, last access 12 November 2020). AIS data for all ships sailing between 54°N, 11.5°E and 55.5°N, 16°E in the measurement period (26 June – 2 July 2018) was acquired from the German Federal Waterways and Shipping Administration in anonymized form, analyzed and filtered by custom software on Matlab platform. ~~Small vessels below 60 m length were excluded.~~

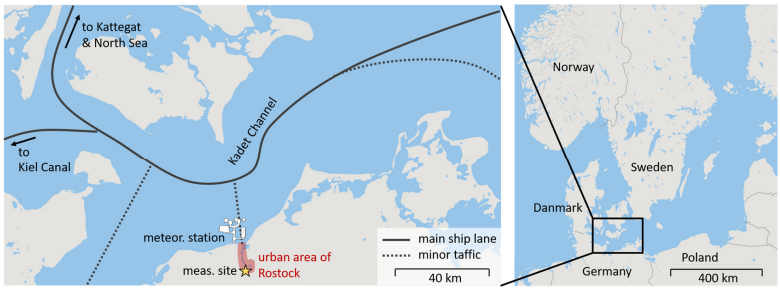

Figure 1: Overview map of the region illustrating the major ship lanes and the position of the measurement site and the meteorological station providing the wind data. A more detailed map can be found in Fig. ~~6~~5.

3 Results and Discussion

~~Before focusing on particles from residual fuel combustion, we characterize the overall particle ensemble and meteorological situation that represent a typical scenario for a North-European coastal region during summer.~~

3.1 ~~Main particle classe~~ Chemical profile of residual fuel emission particles ~~s~~

During 26 June – 2 July 2018, a total number of 290,144 particles were detected by the SPMS instrument, 162,288 particles yielded mass spectra and were sized and chemically analyzed. The ART-2a algorithm produced 715 particle clusters, whereof

Feldfunktion geändert

Formatiert: Hervorheben

Formatiert: Hervorheben

the top 300 clusters accounting for >90 % of the particles were visually inspected. Similar clusters, based on the ion signal of key species were grouped by hand into six general categories. ~~Such groups have variations among their clusters, but similar signatures of the same overall chemical species as well as comparable temporal trends and size distributions. The labelling scheme reflects the most intense peaks and characteristic species for the respective general particle type and is frequently used in the literature (Ault et al., 2010; Decesari et al., 2014; Dall`Osto et al., 2016; Arndt et al., 2017). Peaks are assigned with respect to the most probable ions for a given m/z ratio.~~ The mass spectra of the six general particle classes can be found in the Supplement, Fig. S1, as well as the discussion on it. Here we focus on the class of ship emission particles.

~~The mass spectral signatures of all 300 inspected clusters as well as time series of their particle counts are provided in the Supplement, the attribution to general classes is documented by Table S1.~~

~~Six general particle types were identified. Their particle number and aerodynamic size can be found in Fig. 2(a), whereas average mass spectra of anions and cations are shown in Fig. 2(b) and (c), respectively. Carbon-containing particles contributed the majority to total particle numbers. Their spectra are either dominated by strong carbon cluster peaks from elemental carbon (EC), or by molecular fragments from organic carbon (OC). The balance between these signatures indicate the EC/OC ratio (Ferge et al., 2006; Spencer and Prather, 2006), however, in the present study this ratio is a continuum, broken into several small clusters by ART-2a (Zhou et al., 2006) and manually merged according to their dominant signals.~~

~~The EC-OC particle class shows no distinct K^+ peak, indicating fossil fuel combustion (oil burning or traffic) as most likely source. It has been shown that secondary material increases the particle's hygroscopicity (Moffet et al., 2008)(Ault et al., 2010; Decesari et al., 2014), suppressing the formation of negative ions (Neubauer et al., 1998; Hatch et al., 2014). The strong sulfate signal and the frequent absence of negative carbon clusters indicate condensation of sulfate during atmospheric transport, while its dominance over nitrate can result from processing in marine environment (Ault et al., 2010; Köllner et al., 2017), but also from the summer weather conditions due to the higher volatility of ammonium nitrate compared to ammonium sulfate (Querol et al., 2009; Arndt et al., 2017).~~

~~Particles with molecular fragment signals dominating over the carbon clusters were assigned to the OC-EC class. They also show a pronounced K^+ peak and nitrogen containing signals; both can be attributed to a higher contribution of biomass combustion (Silva et al., 1999; Pagels et al., 2013).~~

~~In the K-CN class, K^+ signals dominate the cation mass spectra, a well-documented signature for aerosols from biomass burning and wood combustion (Silva et al., 1999; Zhang et al., 2013). Potassium has a low ionization energy and the ion is energetically preferred compared to ions of other species, thus it survives collisions in the particle plume, when other ions are neutralized (Reinard and Johnston, 2008). The mass spectra of negative ions show CN^- and CNO^- signals from nitrogen-containing organic compounds (Silva et al., 1999; Köllner et al., 2017).~~

~~A particle class similar to the K-CN particles, but with higher peaks from NO_2^- and NO_3^- indicate a strong contribution of secondary material, including nitrate in addition to the sulfate.~~

~~Sea salt particles are typically larger and produce characteristic signatures. Fresh sea salt particles are characterized by sodium ions (e.g. $^{23}Na^+$, $^{46}NaC^+$, $^{62}Na_2O^+$, $^{63}Na_2OH^+$), K^+, $^{16}O^-$ and $^{35,37}Cl^-$ (Dall'Osto et al., 2004; Murphy et al., 2019). Chlorine is~~

Feldfunktion geändert
Feldfunktion geändert
Feldfunktion geändert
Feldfunktion geändert
Feldfunktion geändert
Feldfunktion geändert
Feldfunktion geändert
Feldfunktion geändert
Feldfunktion geändert
Feldfunktion geändert

~~replaced by nitrate during atmospheric processing (Gard et al., 1998), thus the strong nitrate signals and weak chlorine peaks ($^{35,37}Cl^-$) suggest that these particles are not fresh but have been transported over some distance.~~

~~The~~ The combination of signals from the transition metals V, Fe and Ni is a well-documented marker for particles from residual fuel combustion on ships (Healy et al., 2009; Ault et al., 2010; Xiao et al., 2018; Furutani et al., 2011; Reinard et al., 2007), see Fig. 2 for the mass spectrum. The ~~peak~~ relative peak intensities do not reflect the mass concentration of these species and further metals such as Zn and Cu are less frequently detected in SPMS, despite their high concentration in the fuels and particles (Viana et al., 2009; Popovicheva et al., 2012; Moldanová et al., 2009; Streibel et al., 2017; Corbin et al., 2018). ~~The mechanisms and interactions that affect the ion formation in LDI are not understood in full detail (Reinard and Johnston, 2008; Hatch et al., 2014), however, recently we could show that the light absorption of free atoms in the particle plume can play an important role (Passig et al., 2020).~~ In previous studies on ship emissions, Vanadium signals dominated largely over Fe and Ni peaks (Healy et al., 2009; Ault et al., 2010), and were partly treated as a singular marker (Xiao et al., 2018). ~~However, particularly in an ion marker-based approach, $^{51}V^+$ and $^{67}VO^+$ can interfere with major organic fragments (and $^{56}Fe^+$ with $^{56}CaO^+$).~~ Of note, the KrF-excimer laser used in our experiment resonantly ionizes particle-bound Fe, enabling a more efficient and secure detection of iron (Passig et al., 2020). This allows us to strengthen the assignment by counting only particle clusters to the V-Fe-Ni class that show either the complete peak pattern of $^{51}V^+$, $^{56}Fe^+$, $^{58}Ni^+$, $^{67}VO^+$ or $^{51}V^+$, $^{54}Fe^+$, $^{56}Fe^+$, $^{67}VO^+$. ~~This allows us to strengthen the assignment by counting only particle clusters to the V-Fe-Ni class that show either the complete peak pattern of $^{51}V^+$, $^{56}Fe^+$, $^{58}Ni^+$, $^{62}VO^+$ or $^{51}V^+$, $^{54}Fe^+$, $^{56}Fe^+$, $^{62}VO^+$.~~

Beyond the transition metals from residual fuel combustion, the V-Fe-Ni particles reveal Ca^+ ions that can be attributed to additives of lubrication oil (Toner et al., 2006; Spencer et al., 2006), minor signals from EC and OC as well as a particularly intense $^{97}HSO_4^-$ peak. Considering ~~that also the other particle classes show~~ a strong $^{97}HSO_4^-$ signal also from other particle classes (compare Fig. S1), the sulfate can be primary and secondary.

Apart from the ~~aged~~ sea salt, the particles of all classes show comparable sizes, peaking around 400 – 500 nm~~es~~, see Fig. S12~~(~~a). One explanation lies in the ~~instrumental~~ setup: The optical detection of particles based on Mie scattering ~~is most effective for particle sizes that roughly match the laser wavelength (here 532 nm) and~~ drops rapidly approaching the Rayleigh limit around ~~below about~~ 150 nm (for 532 nm scattering wavelength) (Gaie-Levrel et al., 2012). Furthermore, t~~T~~he aerosol concentrator is optimized for particles of ~~about~~ 2.5 – 10 µm size (Romay et al., 2002) ~~and most likely ineffective for particles smaller than 0.5 µm~~. While detailed data on its performance for small particles is not available, we could estimate an approximately ten-fold concentration for 0.5 µm particles and particle losses of at least 50% below 0.5 µm in a previous study (Passig et al., 2020). Beyond the instrumental aspect, particles in the accumulation mode can be dominant~~te the size distribution in remote areas, and also~~ if local emissions are of minor importance or if they rapidly grow, e.g. by condensation of secondary material.

~~have the longest residence time in the atmosphere and are transported over large distances (Seinfeld and Pandis, 2016). They can dominate the size distribution in remote areas, and also if local emissions are of minor importance or if they rapidly grow, e.g. by condensation of secondary material.~~

Feldfunktion geändert: replaced by nitrate during atmospheric processing (Gard et al., 1998), thus the strong nitrate signals and weak chlorine peaks ($^{35,37}Cl^-$) suggest that these particles are not fresh but have been transported over some distance.
Feldfunktion geändert: The combination of signals from the transition metals V, Fe and Ni is a well-documented marker for particles from residual fuel combustion on ships (Healy et al., 2009; Ault et al., 2010; Xiao et al., 2018; Furutani et al., 2011; Reinard et al., 2007),
Formatiert: Nicht Hervorheben
Feldfunktion geändert: see Fig. 2 for the mass spectrum. The peak relative peak intensities do not reflect the mass concentration of these species and
Feldfunktion geändert: The mechanisms and interactions that affect the ion formation in LDI are not understood in full detail (Reinard and Johnston, 2008; Hatch et al., 2014), however, recently we could show that the light absorption of free atoms in the particle plume can play an important role (Passig et al., 2020).
Feldfunktion geändert: However, particularly in an ion marker-based approach, $^{51}V^+$ and $^{67}VO^+$ can interfere with major organic fragments (and $^{56}Fe^+$ with $^{56}CaO^+$).
Feldfunktion geändert: This allows us to strengthen the assignment by counting only particle clusters to the V-Fe-Ni class that show either the complete peak pattern of $^{51}V^+$, $^{56}Fe^+$, $^{58}Ni^+$, $^{67}VO^+$ or $^{51}V^+$, $^{54}Fe^+$, $^{56}Fe^+$, $^{67}VO^+$.
Feldfunktion geändert: Beyond the transition metals from residual fuel combustion, the V-Fe-Ni particles reveal Ca^+ ions that can be attributed to additives of lubrication oil (Toner et al., 2006; Spencer et al., 2006), minor signals from EC and OC as well as a particularly intense $^{97}HSO_4^-$ peak. Considering that also the other particle classes show a strong $^{97}HSO_4^-$ signal also from other particle classes (compare Fig. S1), the sulfate can be primary and secondary.
Feldfunktion geändert: Apart from the aged sea salt, the particles of all classes show comparable sizes, peaking around 400 – 500 nm~~es~~, see Fig. S12~~(~~a). One explanation lies in the instrumental setup: The optical detection of particles based on Mie scattering is most effective for particle sizes that roughly match the laser wavelength (here 532 nm) and drops rapidly approaching the Rayleigh limit around below about 150 nm (for 532 nm scattering wavelength) (Gaie-Levrel et al., 2012). Furthermore, t~~T~~he aerosol concentrator is optimized for particles of about 2.5 – 10 µm size (Romay et al., 2002) and most likely ineffective for particles smaller than 0.5 µm. While detailed data on its performance for small particles is not available, we could estimate an approximately ten-fold concentration for 0.5 µm particles and particle losses of at least 50% below 0.5 µm in a previous study (Passig et al., 2020). Beyond the instrumental aspect, particles in the accumulation mode can be dominant~~te the size distribution in remote areas, and also~~ if local emissions are of minor importance or if they rapidly grow, e.g. by condensation of secondary material.
Feldfunktion geändert: have the longest residence time in the atmosphere and are transported over large distances (Seinfeld and Pandis, 2016). They can dominate the size distribution in remote areas, and also if local emissions are of minor importance or if they rapidly grow, e.g. by condensation of secondary material.

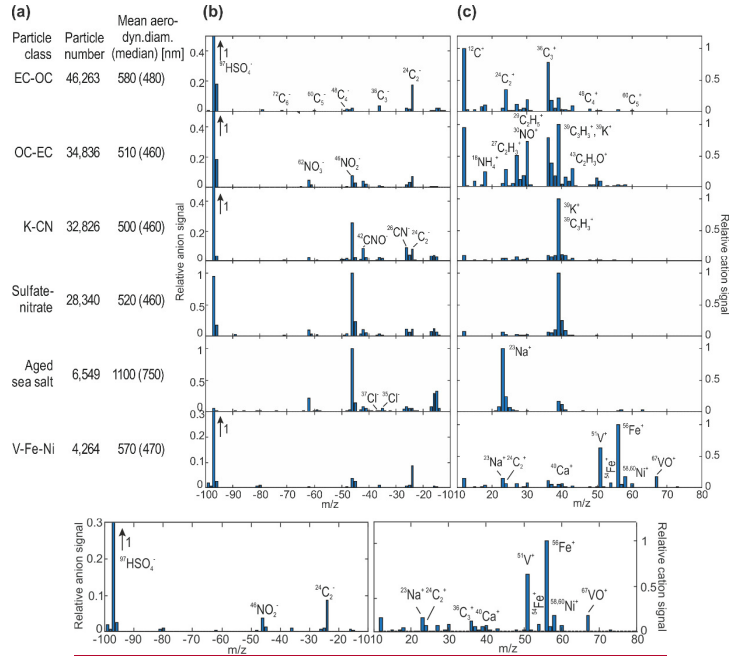

Figure 2: ~~(a) General particle classes, their respective particle numbers and aerodynamic size. (b)~~ **Average anion mass spectra** (left) **and** ~~(c)~~ **cation mass spectra** (right) **of** residual fuel emission particles~~the particle classes~~**. The** ~~mass spectra of~~other particle classes are shown in the Supplement Fig. S1, **the top 300 particle clusters from ART-2a analysis are shown in** Figs. S5 and S6. ~~the Supplement and their assignment to the general classes is documented by Table S1.~~

~~**3.2 Time series of main particle classes and air mass history**~~~~This allows us to strengthen the assignment by counting only particle clusters to the V-Fe-Ni class that show either the complete peak pattern of $^{51}V^+$, $^{56}Fe^+$, $^{58}Ni^+$, $^{67}VO^+$ or $^{51}V^+$, $^{54}Fe^+$, $^{56}Fe^+$, $^{67}VO^+$.~~**3.2 Temporal profile of residual fuel emission particles**

The measurements were performed during a period of relatively calm summer weather with light to moderate winds from mostly northern to eastern directions, representing a typical scenario for a North-European coastal region during summer. The mean PM 2.5 mass was 4.0 µg/cm^3 and the mean particle number density was 44 cm^{-3} (0.25–32 µm), as measured by a monitoring station near the coast line (Grimm EDM-180, http://www.lung.mv-regierung.de/umwelt/luft/akt_wahl.htm). ~~In order to improve the clarity,~~ Fig. 3(a) lists the regions passed by the air masses within the last 24h before arriving at the sampling site, while the ~~detailed~~ back trajectories are shown in Figs. ~~S2~~ S4~~and S3~~. ~~Most of the trajectories passed open sea and sparsely populated regions before reaching the nearby coastal waters and finally the sampling site.~~ The last hour of ~~the~~

Formatiert: Zentriert

Formatiert: Nicht Hervorheben

Formatiert: Hervorheben

~~trajectories~~air transport before arriving at the site can be determined from the local wind data. ~~, recorded at the coastline 12 km north of the site, see Fig. 3(b).~~ Air masses~~After~~ crossing the heavily trafficked ship lanes >20 km north off the coast (see Fig. 1) ~~the air~~ enter~~s~~ the site ~~either directly from the north~~ passing the urban area of Rostock~~, or from eastern directions passing rural regions with forests and agricultural areas.~~

. The wind data (Fig. 3(b)) reveal a pronounced land/onshore circulation, with regularly northern winds in the afternoon and light winds from different directions in the night and morning hours. Fig. 3(c) shows time series of the particle numbers within the general particle classes, while Fig. 3(d) shows their relative contribution to total particle numbers, both with 10 min resolution.

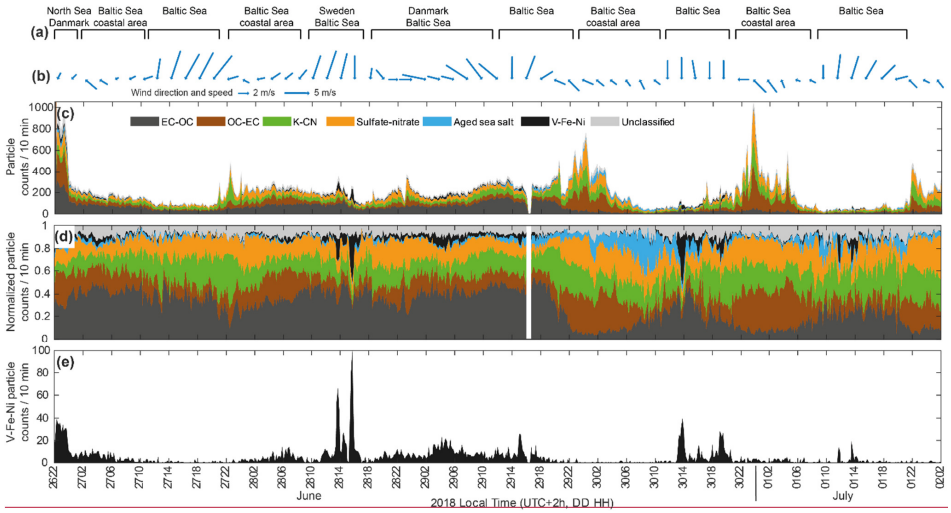

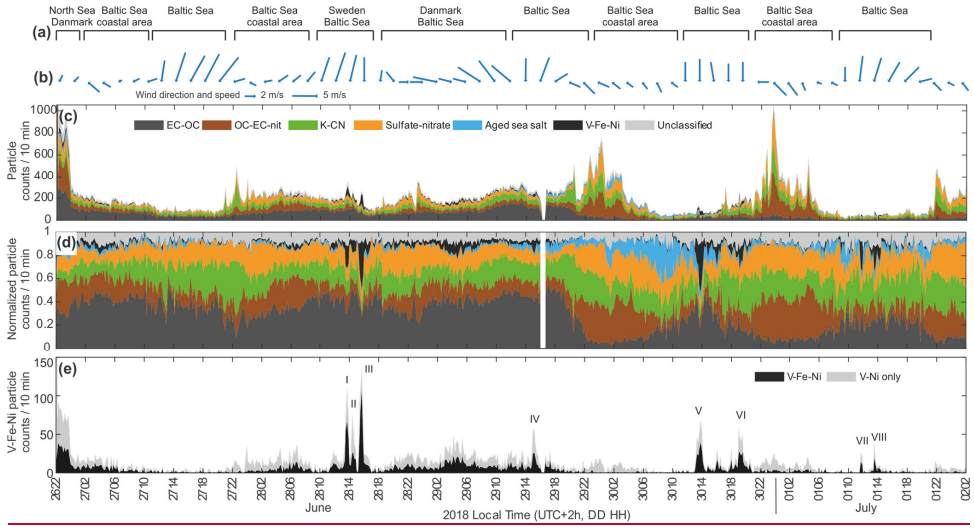

Figure 3: (a) Air mass origin (top row: >12 h, bottom row <12 h) according to the HYSPLIT back trajectory analysis (Fig. ~~S2~~ S4~~and S3~~). (b) Measured wind data from the meteorological station at the harbor exit, 12 km north of the measurement site. (c) The time series of particle counts from the general particle classes shows regional/long-range transported air pollution (26-29 June) and night-time secondary organic aerosol formation (29 June – 02 July), see Supplement for a detailed discussion. (d) The same data as (c), but normalized to total particle counts illustrate the contribution of each particle type ~~as well as increased sea-salt levels during the 30 June~~. (e) The temporal behavior of V-Fe-Ni particles (black) from residual fuel combustion reveals transient events (ship plumes I–VIII) and smooth background signals, predominantly during onshore winds. Apart from the short events, their contribution to total particle numbers is low. The plumes can also be recognized by evaluating only the presence of $^{51}V^+$ and $^{67}VO^+$ (grey area, relative peak area of $^{51}V^+$>5% and $^{67}VO^+$>0%), however with some false positive results from interference with fragments, especially during events with high counts of organic aerosols.

Formatiert: Hervorheben

Formatiert: Nicht Hochgestellt/ Tiefgestellt

Formatiert: Nicht Hochgestellt/ Tiefgestellt

~~The wind data (Fig. 3(b)) reveal a pronounced land/onshore circulation, with regularly northern winds in the afternoon and light winds from different directions in the night and morning hours. Fig. 3(c) shows time series of the particle numbers within the general particle classes, while Fig. 3(d) shows their relative contribution to total particle numbers, both with 10 min resolution.~~

~~The EC-OC particle numbers (dark grey area) exhibit a weak diurnal oscillation, however, not with enhanced levels during the morning and afternoon as expected from increased local traffic and human activity. In contrast, they follow the changes in wind direction and speed. It is conceivable that the northern winds transport local emissions from the city center to the sampling site, however, the strong sulfate peaks in the EC-OC group and the lack of negative ions point on aged particles that might have been transported over larger distances, see Fig. 2. Also the particle size is larger than typical for urban traffic emissions (Dall`Osto et al., 2016) which is in agreement with the assumption that these freshly emitted particles are underrepresented compared to the larger ones that are enriched by the aerosol concentrator.~~

~~The OC-EC-, K-Cn and Sulfate-nitrate particles roughly follow the trend of the EC-OC particles, but show an additional diurnal variation that is especially pronounced during the last two days of the measurements. Their particle numbers increase after sunset and drop in the morning, reflecting condensation of semi-volatile components at night. This temporal behavior is comparable for OC-EC, K-CN and Sulfate-Nitrate particles, because: (I) They are all composed of organic matter to some extend. (II) They can simultaneously grow into the efficiently detected size mode by condensation of secondary material, and (III) all possible diurnal features of aerosol chemistry, such as daytime photochemical formation of SOA or increases in nitrate with relative humidity (Salcedo et al., 2006; Dall'Osto et al., 2009; Healy et al., 2012) are interfered by the strong land/onshore circulation. This dominance of air circulation over local atmospheric chemistry is also reflected by the pronounced particle number maxima during the last nights of the measurement period, where local terrestrial air masses contribute. In contrast, during the second and third night, the air trajectories passed over less land before entering the site and the maxima are substantially smaller. Also the OC-EC and K-CN particle numbers follow the diurnal trend, probably because they grow by night-time condensation into the size mode that is enriched by the aerosol concentrator, while local emissions of smaller particles are barely detected. However, a small transient feature of K-CN particles can be noticed at the 29th June at 8 pm, before the general increase after sunset around 10 pm. It might be associated with local emissions, e.g. from barbecuing. The enhanced contributions of aged sea salt at the 30th June can be attributed to stronger winds in the central Baltic Sea.~~

In the following, we discuss only t~~T~~he mass spectra and time series of V-Fe-Ni particles, for all other classes we refer to the supplement. The V-Fe-Ni particles (Fig. 3(e)) resembles the temporal profile of the ECOC particles, however, with additional transient features that have ~~. These features have~~ a width of approximately 20–60 min and occur only during wind from the North. As apparent from Fig. 3(d), the V-Fe-Ni class contributes only a small fraction to total particle numbers, ~~however~~ while, during the transient events ~~these contribution~~they account~~s~~ for 10–20 %.

In order to give an estimate on the benefit of resonant Fe ionization we performed laboratory experiments on a research ship engine. Herein, we compared the SPMS spectra and the fraction of particles showing metal signatures for the resonant Fe ionization at 248 nm versus the more common SPMS wavelength at 266 nm. The results are shown in the Supplement, Fig. S3. Although these are no ambient air experiments on real plumes, the results indicate an ≈15 times more frequent detection of Fe at 248 nm, which roughly corresponds to the Fe enhancements found in the ambient air study (Passig et al., 2020). Of note, V is ≈2 times and Ni ≈4 times more frequently detected, see Fig. S3. An explanation can be found in the relatively broad laser spectrum at 248 nm overlapping with further atomic absorption lines of the metals (Passig et al., 2020).

The particle identification via ART-2a clustering that recognizes the full pattern of V, Ni and Fe can be evaluated by a comparison with an ion-marker screening for only $^{51}V^+$ and $^{67}VO^+$, as shown by the grey area in Fig. 3(e). $^{51}V^+$ and $^{67}VO^+$ may interfere with major organic fragments (and $^{56}Fe^+$ with $^{56}CaO^+$), as apparent for periods with high contributions from organic particles in Fig. 3. Higher signal thresholds for marker ions can mitigate that problem, on the costs of sensitivity.

~~3.3 Chemical and temporal profiles of residual fuel emission particles~~

~~In order to elucidate the sources and atmospheric processing of the V-Fe-Ni particles, we separately analyzed the mass spectra and temporal behavior of 12 out of the total 15 clusters that were combined to the V-Fe-Ni class. Fig. 4(a) lists the clusters according to their labels in the full cluster analysis (1st row in Fig. 4(a), see Supplement) in the order of their respective particle numbers (2nd row). The mass spectra (Fig. 4(b) and (c)) show signals from EC, OC, Ca^+ and Na^+, see section 3.1 as well as the metal signatures that were used as markers for residual fuel combustion. Generally, all clusters with negative ion spectra reveal a dominant $^{97}HSO_4^-$ peak (with additional EC signals for cluster 161 and 164 and nitrate for cluster 226).~~

Formatiert: Überschrift 2

3.3.~~1~~ Background particles and particles from transient events

To elucidate the sources and atmospheric processing of the V-Fe-Ni particles, we separately analyzed the mass spectra and temporal behavior of the 12 most abundant clusters out of the total 15 clusters assigned to the V-Fe-Ni class. Fig. 4(a) lists the clusters according to their labels in the full cluster analysis (1st row) in the order of their respective particle counts (2nd row). The average mass spectra of the clusters (Fig. 4(b) and (c)) show signals from EC, OC, Ca^+ and Na^+, as well as the metal signatures. Generally, all clusters with negative ion spectra reveal a dominant $^{97}HSO_4^-$ peak (with additional EC signals for cluster 161 and 164 and nitrate for cluster 226).

Time series of the particle clusters are depicted in Fig. 4(d). An important finding here is that the cluster algorithm was exclusively applied to chemical particle data, but it also yielded two distinct groups according to the particle's temporal behavior, as discussed in the following.

The first group of V-Fe-Ni particles, comprising the clusters 97, 111, 127, 138, 196 and 226 shows rather smooth time series, comparable to the EC-OC class in Fig. ~~2~~3(c). The mass spectra of this group reveal either no negative ions or comparable small signals from sulfate (4th row in Fig. 4(a)) or secondary nitrate (cluster 226). Also, the positive ion signals apart from transition metals are weak. The smooth temporal behavior (Fig. 4(d)) gives rise to the term 'background group'. These particles are predominantly observed during phases of light on-shore winds, also from North-Western directions, where heavily trafficked ship routes towards the North Sea and the Atlantic Ocean are located. Such particles most likely origin from distant ~~sections of the~~ shipping lanes ~~or distant regions~~.

The second group identified by mass spectral signatures contributes the transient events and is formed by the clusters 110, 150, 151, 161, 164 and 183. All of these particle clusters show negative ions and, with the exception of cluster 150, also remarkable signals of EC, OC, Ca^+ and Na^+ in the positive ion mass spectra. We term these particles the "transient group", as their temporal behavior point on individual, less distant sources. Cluster 111 combines both properties. Because of the biased aerosol concentration and sampling in our study, the particle size distribution is rather uniform and allows no differentiation between local and distant emissions.

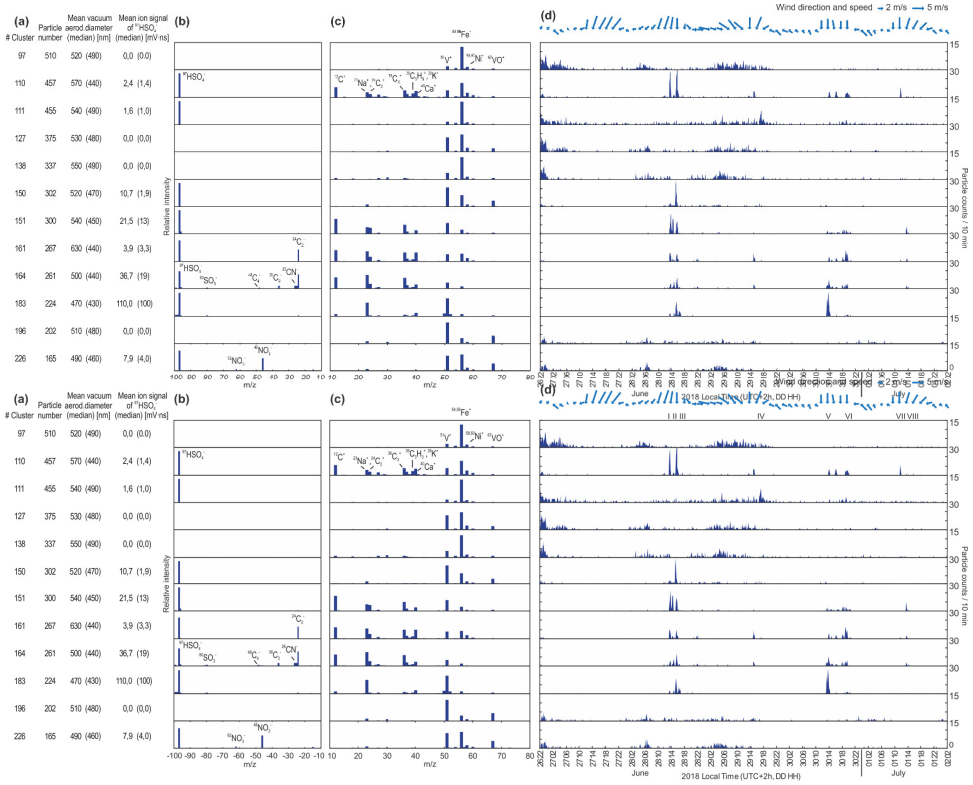

Figure 4: Results of the ART-2a clustering for 12 of the 15 clusters showing signatures of residual fuel combustion. (a) Cluster number according to their labels in the full cluster analysis (see Supplement), particle number, vacuum aerodynamic diameter and average sulfate signal of the clusters. (b) Weight matrices (spectra of the cluster center) of negative ions and (c) positive ions corresponding to average mass spectra. (d) top: measured wind data and ship plume numbers; below: time series of particle counts with 10 min resolution. Note the different y-axis scales. While only mass spectral data was considered in the clustering algorithm, also the time series of the resulting clusters reveal two distinct groups: The transient group with bipolar mass spectra and short events as well as the background group with dominant metal signatures and smooth time series.

~~3.3.2 Mass spectral signatures for ageing of V-Fe-Ni particles~~

The main difference between ~~the mass spectral signatures of the background~~the two groups ~~and the transient group~~ is the limited number of negative ion signals and the weaker positive signatures from EC, OC, Ca^+ and Na^+ for the background

particles. The absence of negative ion signals ~~was often reported for~~in SPMS ~~studies on ambient air~~ was commonly~~and is~~ associated with water uptake during aerosol ageing (Neubauer et al., 1998; Moffet et al., 2008; Ault et al., 2010). but. ~~Particles can acquire low- and semi-volatile material, e.g. ammonium sulfate or nitrate and organic species by condensation, coagulation or heterogeneous reactions (Seinfeld and Pandis, 2016). The increasing hygroscopicity and water uptake predominantly affects the formation of negative ions (Neubauer et al., 1998), but~~ also suppression effects on positive ions were documented (Neubauer et al., 1997; Dall'Osto et al., 2006). Hatch et al. (2014) found that laser absorption and particle ablation in LDI are reduced from coatings of secondary species, finally affecting mass spectra for both polarities~~ (Hatch et al., 2014).~~ s (Hatch et al., 2014). ~~Also charge-transfer reactions in the plume play an important role, because they favour cations with low ionization potential and anions with high electron affinity (Reinard and Johnston, 2008). As an example, K^+ dominates the positive spectrum of wood combustion particles, see e.g. Fig. 2.~~

Previous studies on ship emission particles have discussed the lack of negative ion mass spectra (Ault et al., 2009), ~~and~~ the balance between sulfate and nitrate (Liu et al., 2017) or solely the presence of nitrate signals (Wang et al., 2019) as indicators for atmospheric ageing ~~of ship emission particles~~. However, a suppression of positive ions through ageing was not reported in these studies, although the mass spectra of substantially aged ship particles shown by Ault et al. (2009) ~~(Ault et al., 2009)~~ also reveal a low relative intensity of EC, OC, Ca^+ and Na^+ compared to the freshly emitted particles documented by in-port~~/near-port~~ studies (Healy et al., 2009; Ault et al., 2010; Liu et al., 2017; Xiao et al., 2018). Generally, the formation of negative ions by electron capture requires previous generation of positive ions, and is therefore more prone to suppression effects ~~than positive ion generation~~. In consequence, the relative heights of positive ion peaks apart from the transition metals ~~may provide~~should be considered as a further estimate for the amount of ~~secondary species, water uptake and~~ atmospheric ageing of ship particles. The respective mass spectral indicators for ageing of V-Fe-Ni particles are summarized in Table 1.

Table 1: Mass spectral signatures that indicate the degree of ageing for particles from residual fuel combustion.

	Neg. ion mass spectra	Pos. ion mass spectra	References
freshly emitted	EC, high-sulfur fuels: $^{-80}SO_3^-$, dominant $^{-97}HSO_4^-$	V-Fe-Ni, EC, OC, Na, Ca	(Ault et al., 2010; Healy et al., 2009; Xiao et al., 2018; Liu et al., 2017)
moderately aged, local – regional	$^{-97}HSO_4^-$, secondary nitrate	V-Fe-Ni, smaller EC, OC, Na, Ca	(Liu et al., 2017; Arndt et al., 2017; Gaston et al., 2013; Wang et al., 2019), this work
substantially aged, regional – long range	no signals or secondary sulfate, nitrate, methanesulfonate	dominant V-Fe-Ni	(Ault et al., 2009; Furutani et al., 2011; Arndt et al., 2017), this work

Formatiert: Deutsch (Deutschland)
Feldfunktion geändert
Feldfunktion geändert
Feldfunktion geändert
Feldfunktion geändert
Feldfunktion geändert
Feldfunktion geändert
Feldfunktion geändert
Feldfunktion geändert
Formatiert: Nicht Hochgestellt/ Tiefgestellt
Feldfunktion geändert
Feldfunktion geändert

3.4 3.3 Metal signatures of V-Fe-Ni particles

In contrast to anionsnegative ions and EC, OC as well as alkali catieations, the transition metal signals appear to beare more stable and remain also after long-range transport (Furutani et al., 2011; Ault et al., 2009). Although only speculative here, sulfate-driven metals dissolution in the particle coating might be of importance (Fang et al., 2017). A difference to all previous SPMS studies on ship emissions is the strong Fe^+ signal , comparable to the V^+ peak and the remarkably Ni^+ signal in most particles. This can be attributed to the resonant ionization of Fe at 248 nm (Passig et al., 2020). Because of the increased signals for Fe (and possibly Ni) Therefore, it appears feasible to evaluate whether V/Fe signal ratios may be indicative for a specific source, e.g. as a result of different fuel composition (Viana et al., 2009). However, from Fig. 4(c) and (d), it becomes apparent that the same transient events, respective sources, contribute particle clusters with very different V/Fe ratios. On the other hand, these ratios differ not much among the plumes, as summarized in Table 2. Only plume V stands out by higher V^+ signals in relation to the other metals, and also by a particularly high sulfate signal.

Table 2: Ship plumes according to Figs. 3,4&5, their main properties as well as the median of relative signal ratios for metals and sulfate signals.

Ship plume	Peak time	Plume duration (min)	Number of characterized particles	Particle size (nm)	Peak area ratio V/(V+Fe)	Peak area ratio V/(V+Ni)	Peak area ratio Fe/(Fe+Ni)	$^{97}HSO_4^-$ signal / particle (mV·ns)
I	06/28 13:45	45	182	450	0.55	0.64	0.57	0.23
II	06/28 14:30	45	103	470	0.69	0.85	0.70	0.73
III	06/28 15:30	45	276	450	0.56	0.73	0.70	0.33
IV	06/29 15:15	60	119	470	0.48	0.58	0.59	0.40
V	06/30 13:30	45	138	410	0.76	0.88	0.69	2.20
VI	06/30 19:30	45	126	420	0.53	0.59	0.56	0.50
VII	07/01 11:45	30	24	330	0.53	0.56	0.52	1.76
VIII	07/01 14:00	30	37	410	0.60	0.62	0.54	2.51

In general, background particles tend to show larger Fe and lower V signals compared to the transient group, but due to a number of exceptions (clusters 110 and 196) we cannot draw clear conclusions here. Note that the LDI signal strength in SPMS does not necessarily indicate the component's mass concentration. Beyond the transition metals, Ca^+ signals appear in all clusters of the transient group. Strong calcium signals from lubrication oil additives were frequently observed in SPMS studies on diesel engines (Toner et al., 2008; Shields et al., 2007), mainly because of its low ionization potential and high detection efficiency,; and calcium was also found in particulate emissions from ships using residual fuels (Moldanová et al., 2009; Streibel et al., 2017).

Formatiert: Überschrift 2
Feldfunktion geändert
Feldfunktion geändert
Formatiert: Überschrift 3
Formatiert: Schriftart: (Standard) +Textkörper (Times New Roman)
Formatiert ... [5]
Formatiert ... [6]
Formatiert ... [7]
Formatiert: Hochgestellt
Formatiert ... [8]
Formatiert: Tiefgestellt
Formatiert: Hochgestellt
Formatiert ... [9]
Formatiert: Zentriert, Zeilenabstand: einfach
Formatierte Tabelle
Formatiert ... [1]
Formatiert ... [2]
Formatiert ... [3]
Formatiert ... [4]
Formatiert ... [10]
Formatiert ... [11]
Formatiert: Zentriert, Zeilenabstand: einfach
Formatiert ... [12]
Formatiert: Zentriert, Zeilenabstand: einfach
Formatiert ... [13]
Formatiert: Zentriert, Zeilenabstand: einfach
Formatiert ... [14]
Formatiert: Zentriert, Zeilenabstand: einfach
Formatiert ... [15]
Formatiert: Zentriert, Zeilenabstand: einfach
Formatiert ... [16]
Formatiert: Zentriert, Zeilenabstand: einfach
Formatiert ... [17]
Formatiert: Zentriert, Zeilenabstand: einfach
Formatiert ... [18]
Formatiert: Zentriert, Zeilenabstand: einfach
Feldfunktion geändert
Feldfunktion geändert

3.5~~3~~.~~4~~ Sulfate signals

As apparent from the 4th row in Fig. 4(a) there are considerable differences in sulfate signals, both between the clusters of the transient group and between the plumes, see Table 2~~, with highest values for cluster 183~~. Although sulfate can also be secondary, fresh~~ly emitted~~ plumes from sulfur-rich fuel combustion have particular high sulfate contents from gas-particle conversion of SO_2 (Murphy et al., 2009; Ault et al., 2010; Healy et al., 2009). With this regard, the temporal trend of the sulfate ion yield from all particles is plotted in Fig. 5(b) (yellow area), while the time series of all V-~~/~~Fe-~~/~~Ni-particles ~~from Fig. 3(e) is~~ again shown in Fig. 5(a) for comparison. The sulfate yield shows slightly elevated background for marine air during northern winds and some smaller features that are not correlated with the number of V-Fe-Ni particles. However, for some of the transients from V-Fe-Ni particles, we ~~also~~ find coinciding features of sulfate levels within the full particle ensemble. Comparison with the sulfate ion yield from only V-Fe-Ni particles (brown) reveals that this particle type contributes the main fraction of sulfate during these incidents.

Feldfunktion geändert

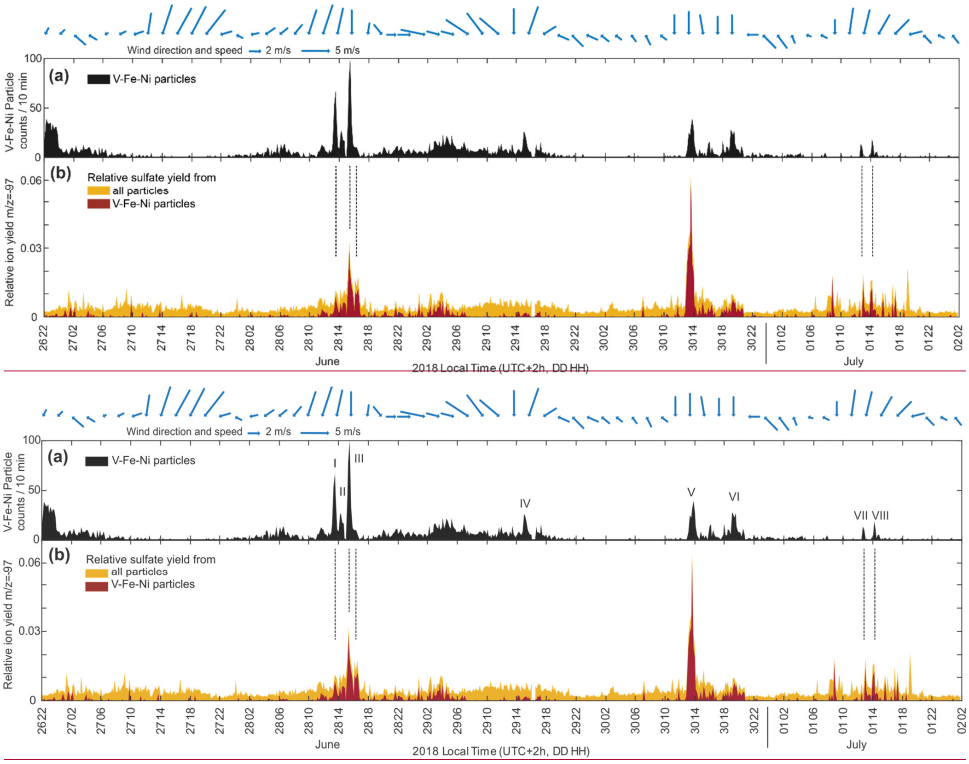

400 **Figure 5: (a) Time series of V-Fe-Ni particles (same as Fig. 3e). (b) Yellow area: The ion yield of HSO_4^- normalized to the particle number per 10 minutes reveals coinciding sulfate events for some of the V-Fe-Ni features. The majority of sulfate is detected on the V-Fe-Ni particles itself (brown area). Most of these particles belong to cluster 183 in Fig. 4.**

3.64 Assignment to ships

Land-based sources can be excluded for the transient group particles, because there are no refineries or chemical industry
405 plants in the town and the local coal power plant was not in operation during measurements. There are two possible source regions of V-Fe-Ni particles: The main shipping lane (Kadet Channel, >50,000 passages per year), about 40 km north of the sampling site and the harbor of Rostock (≈7000 approaches, 75% ferries and roll-on-roll-off ships), located about 10 km north of the site, see Fig. 6(a). The complete Baltic Sea is a SECA, with a 0.1% limit for sulfur in fuel mass. Several studies assessed the compliance of ships to more than 95% (International Transport Forum Policy Papers, 2016; Lähteenmäki-Uutela et al.,
410 2019), thus it is not very likely to detect many ship plumes from operation with conventional high-sulfur bunker fuel within

Feldfunktion geändert

~~the timeframe of~~ about 36h with northern wind in our study. However, an increasing number of ships is currently equipped with scrubbers (Winnes et al., 2018), efficiently removing SO_2 from the exhaust with moderate effects on the PM emissions (Fridell and Salo, 2016; Lehtoranta et al., 2019). Several ships with scrubbers ~~are known to~~ regularly approach the port of Rostock. The ferry route to Denmark is operated with a pair of hybrid ferries (ferry A and B), being ~~. These ships are~~ equipped with scrubbers and usinge batteries for in-port manooeuvring. The diesel engines are started at the harbor exit, ~~when entering open water,~~ directly east of the meteorological station and 12 km north of the measurement site, see the enlarged view in Fig 6(a). On the way back, the engines are stopped at the same position. The typical turnaround time between two departures is 2h and 15 min, matching the delay between two major transient events during afternoon at the 28 June and 30 June, see Fig. 4(d). ~~We analyzed the AIS data to determine the departures and approaches of the ferries within the periods of northern wind.~~ For the period with ~~respective~~ northern-wind~~period~~ at June 28, the times when the ferries pass the harbor exit, where the engines are typically started and stopped, are derived from AIS data, see ~~indicated in~~ Fig. 6(b). These passages of the harbor exit are followed by strong events of particles ~~The time series of particles~~ from the transient group ~~reveal that the strong particle events follow these times~~ with a delay of 45-60 min, in agreement with the wind speed of about 4 m/s. There was a further ferry 'C' with scrubber (no hybrid), approaching Rostock around 12:45 and leaving the port at 14:30 whose signals interfere with ferries A and B. For earlier and later departures and arrivals, the wind direction was unfavourable at this day.

~~Of note, the wind was initially analyzed using the~~From the HYSPLIT back trajectories, ~~as~~ shown by the red and blue lines in Fig. 6(a), ~~). From the blue trajectories, ending 15:00 local time at the measurement site,~~ it appears unlikely that the V-Fe-Ni particle transients stem from the harbor area, as they indicate distant source regions ~~-~~ further east~~along the main shipping route~~. However, there is substantial difference ~~in wind direction~~ between the trajectories and the measured wind data ~~measured at the harbor exit~~, see blue arrows in Fig. 6. Using the measured wind data, the group of transient particle events at 28 June are in agreement with AIS data from the ferries~~, as previously discussed.~~.

On the next day (29 June), there is no transient feature of comparable intensity, because t~~. T~~he wind turned rapidly ~~from North-West~~ to North-East. ~~, and air transport from the harbor to the site was only possible for a short period.~~ However, a broader event, lasting about one hour around 15:00 can be noticed for particles of cluster 111 (Fig. 4). This cluster shows a different chemical profile, with solely sulfate in negative mode and marginal signals of EC, OC and alkali metals in positive mode, ~~indicating~~ what we associated with ~~substantial~~ ageing and a more distant source, see section 3.3~~.2~~. Both the ~~back~~ trajectories as well as the measured wind data shown in Fig. 6(c) reveal a north-eastern direction, guiding air masses from the eastern Kadet channel to the site. Among six cargo ships, ferry C passed this stretch between 12:30 and 14:00 on its way from a different harbor to Sweden. This ferry is also equipped with a scrubber and therefore legally operated with heavy fuel oil, contributing a possible source for the detected V-Fe-Ni particles. Its position at 13:00 is indicated in Fig. 6(c), while the hybrid ferries A and B were in the harbor (engines off) in the relevant time between 14:00 and 15.00 and can therefore be excluded as source ~~for the event~~. Therefore, i~~I~~t appears likely that the event of cluster 111 at 29 June 15:00 results from regional transport from the Kadet channel (>30 km distance). In conjunction with the strong transient signals from the 28 June, this suggests that

Feldfunktion geändert

Feldfunktion geändert

long-range detection of residual fuel operation might be possible if the wind field is captured correctly and if the traffic is not too dense.

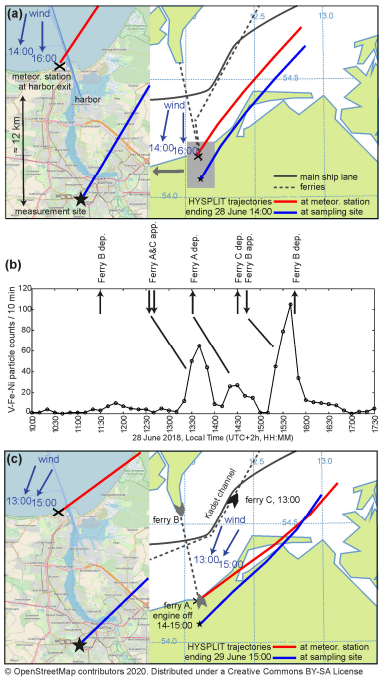

Figure 6: Assignment of transient particle events to distant ship passages. (a) For the first transients, observed on 28 June during a period of northern wind, the HYSPLIT trajectories indicate transport of particles from distant sea areas to the sampling site (star). However, the measured wind directions (blue arrows) in conjunction with ship transponder data reveal ferries with scrubbers as the probable source. (b) Time series of particles from the transient group during northern winds at June 28. The particle events follow the approach and departure times of the ferries (arrows) with a delay of about 45 min during optimum wind directions. (c) On 29 June, the wind direction is north-northeast and only one weak transient event appears (see Fig. 4). However, a broader feature of aged V-Fe-Ni particles at 15:00 indicate a distant source and ferry C is underway in the Kadet channel in the respective timeframe (and six further ships). The difference between trajectories and measured wind data emphasize the importance of accurate meteorological data in potential future monitoring systems.

At 30 June, ~~there was a period of~~during straight north winds, ~~and~~ Fig. 4(d) shows several transient V-Fe-Ni particle events ~~for this time~~, including a small dual peak pattern for cluster 110 with 2 h 15 min delay, matching to AIS-derived departures of ferry A and B, respectively. The time series of sulfate ~~ion~~ signals in Fig. 5(b) reveals a strong increase ~~in sulfate levels~~ that is mainly contributed by particles from cluster 183, compare Fig. 4. The event coincides with ~~the aforementioned event from~~ departure of ferry A and may be associated with scrubber malfunction or delayed onset of its operation. High sulfate emissions

from ships ~~that have~~with installed scrubbers have previously been reported (Mellqvist et al., 2017b; Mellqvist et al., 2017a). However, a different source ~~for the sulfate event~~, such as a further passing ship, cannot be excluded.

The ~~origin of the~~ background particles ~~with V-Fe-Ni~~ signals ~~cannot be attributed to individual ships. They may~~can be associated with general ship traffic, which is also supported by their increase during wind from the western Baltic Sea and the North Sea. The high levels at beginning of the measurements followed a period of air mass stagnation in the western Baltic Sea, where emissions have probably been enriched ~~and were then transported to the site by light winds~~. Ships can emit V-Fe-Ni particles for three reasons: (I) under operation with residual fuels by using scrubbers or (II) if non-compliant fuels or (III) desulfurized hybrid fuels are used. ~~However,~~ Antturi et al. estimated ~~in 2016~~, that only 136 of about 5000 ships sailing in the Baltic Sea had installed a scrubber and the large majority of ships use distillate fuels such as MGO (Antturi et al., 2016). ~~Although scrubbers gain importance, a~~Therefore, a further source is conceivable: As shown in Fig. 4, all particle clusters that belong to the transient group show calcium signals from lubrication oil. While the size distribution of freshly emitted soot particles from diesel engines peaks well below 100 nm (Streibel et al., 2017; Oeder et al., 2015), the majority of particles in the accumulation modes show signatures of ~~lubrication~~ lube oil (Lyyränen et al., 1999; Sakurai et al., 2003; Toner et al., 2006). Because many ships run on residual fuels outside the SECAs and switch to low-sulfur distillates ~~fuels~~ when entering them (Van Roy, W and Scheldemann, K., 2016; Lähteenmäki-Uutela et al., 2019), their lubrication oil ~~can~~ contains metals from previous residual fuel operation that can consequently be emitted in small amounts also during operation in SECAs, as shown by our measurements on a research ship engine, see Supplement. Recently, also Zanatta et al. (2020) found a limited number of V-Fe particles in the marine boundary layer along ship lanes in the Baltic Sea using an aircraft-based ~~SPMS (Zanatta et al., 2020).~~SPMS.

Our analysis of AIS data revealed that a total number of 470 cargo ships, tankers and passenger ships of all sizes were sailing the major ship lane during our measurement period. It should be noted, that the ships running on distillate fuels such as MGO, cannot be separated from other fuel combustion sources by our approach. Considering the typical compliance rate and the small number of ships with scrubbers, it can be estimated that less than 10% of the particles from ships are V-Fe-Ni particles ~~and therefore identified by our approach~~. Consequently, a substantial fraction of the EC-OC particles may also stem from ships, which is supported by the increased number of EC-OC particles during on-shore winds, see Fig. 3.

4. Conclusions

With the present study, we demonstrated the chemical detection of individual ship plumes from more than 10 km distance. It could be shown that also ships with installed scrubbers can be detected by their PM emissions indicating that the emissions of toxic transition metals from residual fuel combustion are not sufficiently abated by scrubbers. This emphasizes the need for additional cleaning technologies and cleaner fuels. By using chemical indicators on a single-particle basis ~~instead of physical indicators~~ for the presence of ship plumes, we extended the approach ~~of Ausmeel et al.~~ to perform stationary measurements at some distance downwind of shipping lanes (Ausmeel et al., 2019; Celik et al., 2020). Of note, this ~~change to chemical indicators~~

Feldfunktion geändert
Feldfunktion geändert
Feldfunktion geändert
Feldfunktion geändert
Feldfunktion geändert
Feldfunktion geändert

renders the method independent from background aerosols, as long as source-specific and detectable markers exist. We analyzed mass spectral signatures for ageing of particles from residual fuel combustion and recommend to consider the suppression of positive ions apart from transition metals as additional ageing indicator for this particle class. Our~~The~~ results furthermore suggest that the signal ratio between transition metals is not a suitable marker for individual ship assignment with SPMS.

From analysis of transient particle events, wind data and ship transponder signals, it becomes apparent that accuracy in wind data, possible mixing of different plumes during high traffic and prevailing wind directions are key limiting factors rather than chemical detection limits or background air pollution. Consequently, SPMS-based monitoring systems should acquire local wind data and small-scale plume dispersion models should be integrated (Matthias et al., 2018; Badeke et al., 2020). The possible operation time is mainly limited by the prevailing wind directions, which should be perpendicular to the ship lane to avoid plume mixing and straight to the monitoring site. However, this limitation can be overcome by installation of ~~multiple~~ two monitoring stations. Favorable places are opposite sides of straits covering the main wind directions, at islands near major shipping routes and waterways to large ports. Mobile ship-based units could complement such monitoring networks.

While our approach can detect ships plumes from residual fuel operation, it is not applicable for monitoring of ship emissions from distillate fuels, because in its present form, it is not unambiguously separating ships running on MGO from land-based traffic emissions. Novel markers for ship emissions beyond the metal signatures have been identified, including source-specific signatures of polycyclic aromatic hydrocarbons (PAH) (Czech et al., 2017a; Czech et al., 2017b). Recent developments in SPMS allow to acquire detailed PAH-profiles from individual particles (Passig et al., 2017; Schade et al., 2019) and therefore they open a perspective towards a comprehensive monitoring protocol for ship emissions and individual plumes.

Feldfunktion geändert

Feldfunktion geändert

Feldfunktion geändert

Data availability. Data are available on request from Johannes Passig (johannes.passig@uni-rostock.de).

Supplement. The supplement related to this article is available online at:

Author contributions. JP designed the experiments, analyzed data, prepared the figures and wrote the manuscript with contributions from all authors. JS and RI developed software and performed the experiments. LL, XL and ZZ provided the SPMS instrument. TA and RZ assisted with technical support, data interpretation and manuscript writing.

Competing interests. The authors declare that they have no conflict of interest.

Acknowledgements. Instrumental and technical support by Photonion GmbH, Schwerin, Germany is gratefully acknowledged. We thank the German Federal Waterways and Shipping Administration for providing AIS data, Germany's National Meteorological Service, 'Deutscher Wetterdienst' for wind data and the State Agency for the Environment, Nature Conservation and Geology Mecklenburg-Vorpommern for PM 2.5 data. The authors gratefully acknowledge the NOAA Air

Resources Laboratory (ARL) for the provision of the HYSPLIT transport and dispersion model and READY website (https://www.ready.noaa.gov, last access: 20 November 2020) used in this publication.

Financial support. This research has been supported by the Deutsche Forschungsgemeinschaft (grant no. ZI 764/6-1), the Bundesministerium für Wirtschaft und Energie (grant no. ZF4402101 ZG7), the Helmholtz-Gemeinschaft (International Lab AeroHealth), and the Helmholtz Virtual Institute of Complex Molecular Systems in Environmental Health (HICE).

References

Antturi, J., Hänninen, O., Jalkanen, J.-P., Johansson, L., Prank, M., Sofiev, M., and Ollikainen, M.: Costs and benefits of low-sulphur fuel standard for Baltic Sea shipping, J. Environ. Manag., 184, 431–440, https://doi.org/10.1016/j.jenvman.2016.09.064, 2016.

Arndt, J., Sciare, J., Mallet, M., Roberts, G. C., Marchand, N., Sartelet, K., Sellegri, K., Dulac, F., Healy, R. M., and Wenger, J. C.: Sources and mixing state of summertime background aerosol in the north-western Mediterranean basin, Atmos. Chem. Phys., 17, 6975–7001, https://doi.org/10.5194/acp-17-6975-2017, 2017.

Ault, A. P., Gaston, C. I., Wang, Y., Dominguez, G., Thiemens, M. H., and Prather, K. A.: Characterization of the single particle mixing state of individual ship plume events measured at the Port of Los Angeles, Environ. Sci. Technol., 44, 1954–1961, https://doi.org/10.1021/es902985h, 2010.

Ault, A. P., Moore, M. J., Furutani, H., and Prather, K. A.: Impact of Emissions from the Los Angeles Port Region on San Diego Air Quality during Regional Transport Events, Environ. Sci. Technol., 43, 3500–3506, https://doi.org/10.1021/es8018918, 2009.

Ausmeel, S., Eriksson, A., Ahlberg, E., Sporre, M. K., Spanne, M., and Kristensson, A.: Ship plumes in the Baltic Sea Sulfur Emission Control Area: chemical characterization and contribution to coastal aerosol concentrations, Atmos. Chem. Phys., 20, 9135–9151, https://doi.org/10.5194/acp-20-9135-2020, 2020.

Ausmeel, S., Eriksson, A., Ahlberg, E., and Kristensson, A.: Methods for identifying aged ship plumes and estimating contribution to aerosol exposure downwind of shipping lanes, Atmos. Meas. Tech., 12, 4479–4493, https://doi.org/10.5194/amt-12-4479-2019, 2019.

Badeke, R., Matthias, V., and Grawe, D.: Parameterizing the vertical downward dispersion of ship exhaust gas in the near-field, Atmos. Chem. Phys. Discuss., 2020, 1–27, https://doi.org/10.5194/acp-2020-753, 2020.

Balzani Lööv, J. M., Alfoldy, B., Gast, L. F. L., Hjorth, J., Lagler, F., Mellqvist, J., Beecken, J., Berg, N., Duyzer, J., Westrate, H., Swart, D. P. J., Berkhout, A. J. C., Jalkanen, J.-P., Prata, A. J., van der Hoff, G. R., and Borowiak, A.: Field test of available methods to measure remotely SO_x and NO_x emissions from ships, Atmos. Meas. Tech., 7, 2597–2613, https://doi.org/10.5194/amt-7-2597-2014, 2014.

Beecken, J., Mellqvist, J., Salo, K., Ekholm, J., and Jalkanen, J.-P.: Airborne emission measurements of SO_2 NO_x and particles from individual ships using a sniffer technique, Atmos. Meas. Tech., 7, 1957–1968, https://doi.org/10.5194/amt-7-1957-2014, 2014.

Berg, N., Mellqvist, J., Jalkanen, J.-P., and Balzani, J.: Ship emissions of SO 2 and NO 2 DOAS measurements from airborne platforms, Atmos. Meas. Tech., 5, 1085–1098, https://doi.org/10.5194/amt-5-1085-2012, 2012.

Celik, S., Drewnick, F., Fachinger, F., Brooks, J., Darbyshire, E., Coe, H., Paris, J.-D., Eger, P. G., Schuladen, J., Tadic, I., Friedrich, N., Dienhart, D., Hottmann, B., Fischer, H., Crowley, J. N., Harder, H., and Borrmann, S.: Influence of vessel characteristics and atmospheric processes on the gas and particle phase of ship emission plumes: in situ measurements in the Mediterranean Sea and around the Arabian Peninsula, Atmos. Chem. Phys., 20, 4713–4734, https://doi.org/10.5194/acp-20-4713-2020, available at: https://acp.copernicus.org/articles/20/4713/2020/, 2020.

Celo, V., Dabek-Zlotorzynska, E., and McCurdy, M.: Chemical Characterization of Exhaust Emissions from Selected Canadian Marine Vessels: The Case of Trace Metals and Lanthanoids, Environ. Sci. Technol., 49, 5220–5226, https://doi.org/10.1021/acs.est.5b00127, 2015.

Chen, G.: An investigation of the chemistry of ship emission plumes during ITCT 2002, J. Geophys. Res., 110, 16,213, https://doi.org/10.1029/2004JD005236, 2005.

Corbett, J. J., Winebrake, J. J., Green, E. H., Kasibhatla, P., Eyring, V., and Lauer, A.: Mortality from Ship Emissions: A Global Assessment, Environ. Sci. Technol., 41, 8512–8518, https://doi.org/10.1021/es071686z, 2007.

Corbin, J. C., Czech, H., Massabò, D., Mongeot, F. B. de, Jakobi, G., Liu, F., Lobo, P., Mennucci, C., Mensah, A. A., Orasche, J., Pieber, S. M., Prévôt, A. S. H., Stengel, B., Tay, L.-L., Zanatta, M., Zimmermann, R., El Haddad, I., and Gysel, M.: Infrared-absorbing carbonaceous tar can dominate light absorption by marine-engine exhaust, npj clim. atmos. sci., 2, 12, https://doi.org/10.1038/s41612-019-0069-5, 2019.

Corbin, J. C., Mensah, A. A., Pieber, S. M., Orasche, J., Michalke, B., Zanatta, M., Czech, H., Massabò, D., Buatier de Mongeot, F., Mennucci, C., El Haddad, I., Kumar, N. K., Stengel, B., Huang, Y., Zimmermann, R., Prévôt, A. S. H., and Gysel, M.: Trace Metals in Soot and PM2.5 from Heavy-Fuel-Oil Combustion in a Marine Engine, Environ. Sci. Technol., 52, 6714–6722, https://doi.org/10.1021/acs.est.8b01764, 2018.

Czech, H., Schnelle-Kreis, J., Streibel, T., and Zimmermann, R.: New directions: Beyond sulphur, vanadium and nickel – About source apportionment of ship emissions in emission control areas, Atmos. Environ., 163, 190–191, https://doi.org/10.1016/j.atmosenv.2017.05.017, 2017a.

Czech, H., Stengel, B., Adam, T., Sklorz, M., Streibel, T., and Zimmermann, R.: A chemometric investigation of aromatic emission profiles from a marine engine in comparison with residential wood combustion and road traffic: Implications for source apportionment inside and outside sulphur emission control areas, Atmos. Environ., 167, 212–222, https://doi.org/10.1016/j.atmosenv.2017.08.022, 2017b.

Dall'Osto, M., Harrison, R. M., Beddows, D. C. S., Freney, E. J., Heal, M. R., and Donovan, R. J.: Single-Particle Detection Efficiencies of Aerosol Time-of-Flight Mass Spectrometry during the North Atlantic Marine Boundary Layer Experiment, Environ. Sci. Technol., 40, 5029–5035, https://doi.org/10.1021/es050951i, 2006.

Di Wu, Li, Q., Ding, X., Sun, J., Li, D., Fu, H., Teich, M., Ye, X., and Chen, J.: Primary Particulate Matter Emitted from Heavy Fuel and Diesel Oil Combustion in a Typical Container Ship: Characteristics and Toxicity, Environ. Sci. Technol., 52, 12943–12951, https://doi.org/10.1021/acs.est.8b04471, 2018.

Diesch, J.-M., Drewnick, F., Klimach, T., and Borrmann, S.: Investigation of gaseous and particulate emissions from various marine vessel types measured on the banks of the Elbe in Northern Germany, Atmos. Chem. Phys., 13, 3603–3618, https://doi.org/10.5194/acp-13-3603-2013, available at: https://acp.copernicus.org/articles/13/3603/2013/, 2013.

Eyring, V., Isaksen, I. S., Berntsen, T., Collins, W. J., Corbett, J. J., Endresen, O., Grainger, R. G., Moldanova, J., Schlager, H., and Stevenson, D. S.: Transport impacts on atmosphere and climate: Shipping, Atmos. Environ., 44, 4735–4771, https://doi.org/10.1016/j.atmosenv.2009.04.059, 2010.

Fang, T., Guo, H., Zeng, L., Verma, V., Nenes, A., and Weber, R. J.: Highly Acidic Ambient Particles, Soluble Metals, and Oxidative Potential: A Link between Sulfate and Aerosol Toxicity, Environ. Sci. Technol., 51, 2611–2620, https://doi.org/10.1021/acs.est.6b06151, 2017.

Fridell, E. and Salo, K.: Measurements of abatement of particles and exhaust gases in a marine gas scrubber, Proceedings of the IMechE, 230, 154–162, https://doi.org/10.1177/1475090214543716, 2016.

Furutani, H., Jung, J., Miura, K., Takami, A., Kato, S., Kajii, Y., and Uematsu, M.: Single-particle chemical characterization and source apportionment of iron-containing atmospheric aerosols in Asian outflow, J. Geophys. Res., 116, https://doi.org/10.1029/2011JD015867, 2011.

Gaie-Levrel, F., Perrier, S., Perraudin, E., Stoll, C., Grand, N., and Schwell, M.: Development and characterization of a single particle laser ablation mass spectrometer (SPLAM) for organic aerosol studies, Atmos. Meas. Tech., 5, 225–241, https://doi.org/10.5194/amt-5-225-2012, 2012.

Gaston, C. J., Quinn, P. K., Bates, T. S., Gilman, J. B., Bon, D. M., Kuster, W. C., and Prather, K. A.: The impact of shipping, agricultural, and urban emissions on single particle chemistry observed aboard the R/V Atlantis during CalNex, J. Geophys. Res., 118, 5003–5017, https://doi.org/10.1002/jgrd.50427, 2013.

Hatch, L. E., Pratt, K. A., Huffman, J. A., Jimenez, J. L., and Prather, K. A.: Impacts of Aerosol Aging on Laser Desorption/Ionization in Single-Particle Mass Spectrometers, Aerosol Sci. Technol., 48, 1050–1058, https://doi.org/10.1080/02786826.2014.955907, 2014.

Healy, R. M., O'Connor, I. P., Hellebust, S., Allanic, A., Sodeau, J. R., and Wenger, J. C.: Characterisation of single particles from in-port ship emissions, Atmos. Environ., 43, 6408–6414, https://doi.org/10.1016/j.atmosenv.2009.07.039, 2009.

International Transport Forum Policy Papers, 2016.

Jonson, J. E., Gauss, M., Schulz, M., Jalkanen, J.-P., and Fagerli, H.: Effects of global ship emissions on European air pollution levels, Atmos. Chem. Phys., 20, 11399–11422, https://doi.org/10.5194/acp-20-11399-2020, 2020.

Jonson, J. E., Gauss, M., Jalkanen, J.-P., and Johansson, L.: Effects of strengthening the Baltic Sea ECA regulations, Atmos. Chem. Phys., 19, 13469–13487, https://doi.org/10.5194/acp-19-13469-2019, 2019.

Kattner, L., Mathieu-Üffing, B., Burrows, J. P., Richter, A., Schmolke, S., Seyler, A., and Wittrock, F.: Monitoring compliance with sulfur content regulations of shipping fuel by in situ measurements of ship emissions, Atmos. Chem. Phys., 15, 10087–10092, https://doi.org/10.5194/acp-15-10087-2015, 2015.

Lack, D. A., Cappa, C. D., Langridge, J., Bahreini, R., Buffaloe, G., Brock, C., Cerully, K., Coffman, D., Hayden, K., Holloway, J., Lerner, B., Massoli, P., Li, S.-M., McLaren, R., Middlebrook, A. M., Moore, R., Nenes, A., Nuaaman, I., Onasch, T. B., Peischl, J., Perring, A., Quinn, P. K., Ryerson, T., Schwartz, J. P., Spackman, R., Wofsy, S. C., Worsnop, D., Xiang, B., and Williams, E.: Impact of Fuel Quality Regulation and Speed Reductions on Shipping Emissions: Implications for Climate and Air Quality, Environ. Sci. Technol., 45, 9052–9060, https://doi.org/10.1021/es2013424, 2011.

Lack, D. A., Corbett, J. J., Onasch, T., Lerner, B., Massoli, P., Quinn, P. K., Bates, T. S., Covert, D. S., Coffman, D., Sierau, B., Herndon, S., Allan, J., Baynard, T., Lovejoy, E., Ravishankara, A. R., and Williams, E.: Particulate emissions from commercial shipping: Chemical, physical, and optical properties, J. Geophys. Res., 114, 4090, https://doi.org/10.1029/2008JD011300, 2009.

Lähteenmäki-Uutela, A., Yliskylä-Peuralahti, J., Repka, S., and Mellqvist, J.: What explains SECA compliance: rational calculation or moral judgment?, WMU J Marit Affairs, 18, 61–78, https://doi.org/10.1007/s13437-019-00163-1, 2019.

Lehtoranta, K., Aakko-Saksa, P., Murtonen, T., Vesala, H., Ntziachristos, L., Rönkkö, T., Karjalainen, P., Kuittinen, N., and Timonen, H.: Particulate Mass and Nonvolatile Particle Number Emissions from Marine Engines Using Low-Sulfur Fuels, Natural Gas, or Scrubbers, Environ. Sci. Technol., 53, 3315–3322, https://doi.org/10.1021/acs.est.8b05555, 2019.

Li, L., Huang, Z., Dong, J., Li, M., Gao, W., Nian, H., Fu, Z., Zhang, G., Bi, X., Cheng, P., and Zhou, Z.: Real time bipolar time-of-flight mass spectrometer for analyzing single aerosol particles, Int. J. Mass Spectrom., 303, 118–124, https://doi.org/10.1016/j.ijms.2011.01.017, 2011.

Liu, Z., Lu, X., Feng, J., Fan, Q., Zhang, Y., and Yang, X.: Influence of Ship Emissions on Urban Air Quality: A Comprehensive Study Using Highly Time-Resolved Online Measurements and Numerical Simulation in Shanghai, Environ. Sci. Technol., 51, 202–211, https://doi.org/10.1021/acs.est.6b03834, 2017.

Lyyränen, J., Jokiniemi, J., Kauppinen, E. I., and Joutsensaari, J.: Aerosol characterisation in medium-speed diesel engines operating with heavy fuel oils, J. Aerosol Sci., 30, 771–784, https://doi.org/10.1016/S0021-8502(98)00763-0, available at: http://www.sciencedirect.com/science/article/pii/S0021850298007630, 1999.

Matthias, V., Arndt, J. A., Aulinger, A., Bieser, J., Denier van der Gon, Hugo, Kranenburg, R., Kuenen, J., Neumann, D., Pouliot, G., and Quante, M.: Modeling emissions for three-dimensional atmospheric chemistry transport models, J. Air Waste Manage., 68, 763–800, https://doi.org/10.1080/10962247.2018.1424057, 2018.

Mellqvist, J., Beecken, J., and Conde, V. Ekholm, J.: Surveillance of sulphur emissions from ships in Danish waters. Report to the Danish Environmental Protection Agency., https://research.chalmers.se/publication/500251, last access: 24 November 2020, 2017a.

Mellqvist, J., Conde, V., Beecken, J., and Ekholm, J.: Fixed remote surveillance of fuel sulfur content in ships from fixed sites in the Göteborg ship channel and Öresund bridge, Report, Chalmers University of Technology, 2017b.

Moffet, R. C., Qin, X., Rebotier, T., Furutani, H., and Prather, K. A.: Chemically segregated optical and microphysical properties of ambient aerosols measured in a single-particle mass spectrometer, J. Geophys. Res., 113, https://doi.org/10.1029/2007JD009393, 2008.

Moldanová, J., Fridell, E., Popovicheva, O., Demirdjian, B., Tishkova, V., Faccinetto, A., and Focsa, C.: Characterisation of particulate matter and gaseous emissions from a large ship diesel engine, Atmospheric Environ., 43, 2632–2641, https://doi.org/10.1016/j.atmosenv.2009.02.008, 2009.

Murphy, S. M., Agrawal, H., Sorooshian, A., Padró, L. T., Gates, H., Hersey, S., Welch, W. A., Jung, H., Miller, J. W., Cocker, D. R., Nenes, A., Jonsson, H. H., Flagan, R. C., and Seinfeld, J. H.: Comprehensive Simultaneous Shipboard and Airborne Characterization of Exhaust from a Modern Container Ship at Sea, Environ. Sci. Technol., 43, 4626–4640, https://doi.org/10.1021/es802413j, 2009.

Neubauer, K. R., Johnston, M. V., and Wexler, A. S.: Humidity effects on the mass spectra of single aerosol particles, Atmos. Environ., 32, 2521–2529, https://doi.org/10.1016/S1352-2310(98)00005-3, 1998.

Neubauer, K. R., Johnston, M. V., and Wexler, A. S.: On-line analysis of aqueous aerosols by laser desorption ionization, Int. J. Mass. Spectrom. Ion Process., 163, 29–37, https://doi.org/10.1016/S0168-1176(96)04534-X, 1997.

Oeder, S., Kanashova, T., Sippula, O., Sapcariu, S. C., Streibel, T., Arteaga-Salas, J. M., Passig, J., Dilger, M., Paur, H.-R., Schlager, C., Mülhopt, S., Diabaté, S., Weiss, C., Stengel, B., Rabe, R., Harndorf, H., Torvela, T., Jokiniemi, J. K., Hirvonen, M.-R., Schmidt-Weber, C., Traidl-Hoffmann, C., BéruBé, K. A., Wlodarczyk, A. J., Prytherch, Z., Michalke, B., Krebs, T., Prévôt, A. S. H., Kelbg, M., Tiggesbäumker, J., Karg, E., Jakobi, G., Scholtes, S., Schnelle-Kreis, J., Lintelmann, J., Matuschek, G., Sklorz, M., Klingbeil, S., Orasche, J., Richthammer, P., Müller, L., Elsasser, M., Reda, A., Gröger, T., Weggler, B., Schwemer, T., Czech, H., Rüger, C. P., Abbaszade, G., Radischat, C., Hiller, K., Buters, J. T. M., Dittmar, G., and Zimmermann, R.: Particulate matter from both heavy fuel oil and diesel fuel shipping emissions show strong biological effects on human lung cells at realistic and comparable in vitro exposure conditions, PloS one, 10, e0126536, https://doi.org/10.1371/journal.pone.0126536, 2015.

Passig, J. and Zimmermann, R.: Laser Ionization in Single-Particle Mass Spectrometry, Wiley Online Books, 359-411, 2021.

Passig, J., Schade, J., Rosewig, E. I., Irsig, R., Kröger-Badge, T., Czech, H., Sklorz, M., Streibel, T., Li, L., Li, X., Zhou, Z., Fallgren, H., Moldanova, J., and Zimmermann, R.: Resonance-enhanced detection of metals in aerosols using single-particle mass spectrometry, Atmos. Chem. Phys., 20, 7139–7152, https://doi.org/10.5194/acp-20-7139-2020, 2020.

Passig, J., Schade, J., Oster, M., Fuchs, M., Ehlert, S., Jäger, C., Sklorz, M., and Zimmermann, R.: Aerosol Mass Spectrometer for Simultaneous Detection of Polyaromatic Hydrocarbons and Inorganic Components from Individual Particles, Anal. Chem., 89, 6341–6345, https://doi.org/10.1021/acs.analchem.7b01207, 2017.

Petzold, A., Hasselbach, J., Lauer, P., Baumann, R., Franke, K., Gurk, C., Schlager, H., and Weingartner, E.: Experimental studies on particle emissions from cruising ship, their characteristic properties, transformation and atmospheric lifetime in the marine boundary layer, Atmos. Chem. Phys., 8, 2387–2403, https://doi.org/10.5194/acp-8-2387-2008, 2008.

Popovicheva, O., Kireeva, E., Persiantseva, N., Timofeev, M., Bladt, H., Ivleva, N. P., Niessner, R., and Moldanová, J.: Microscopic characterization of individual particles from multicomponent ship exhaust, J. Environ. Monit., 14, 3101–3110, https://doi.org/10.1039/c2em30338h, 2012.

Pratt, K. A. and Prather, K. A.: Mass spectrometry of atmospheric aerosols--recent developments and applications. Part II: On-line mass spectrometry techniques, Mass Spectrom. Rev., 31, 17–48, https://doi.org/10.1002/mas.20330, 2012.

Pratt, K. A., Mayer, J. E., Holecek, J. C., Moffet, R. C., Sanchez, R. O., Rebotier, T. P., Furutani, H., Gonin, M., Fuhrer, K., Su, Y., Guazzotti, S., and Prather, K. A.: Development and Characterization of an Aircraft Aerosol Time-of-Flight Mass Spectrometer, Anal. Chem., 81, 1792–1800, https://doi.org/10.1021/ac801942r, 2009.

Reinard, M. S., Adou, K., Martini, J. M., and Johnston, M. V.: Source characterization and identification by real-time single particle mass spectrometry, Atmos. Environ., 41, 9397–9409, https://doi.org/10.1016/j.atmosenv.2007.09.001, 2007.

Romay, F. J., Roberts, D. L., Marple, V. A., Liu, B. Y. H., and Olson, B. A.: A High-Performance Aerosol Concentrator for Biological Agent Detection, Aerosol Sci. Technol., 36, 217–226, https://doi.org/10.1080/027868202753504074, 2002.

Sakurai, H., Tobias, H. J., Park, K., Zarling, D., Docherty, K. S., Kittelson, D. B., McMurry, P. H., and Ziemann, P. J.: On-line measurements of diesel nanoparticle composition and volatility, Atmos. Environ., 37, 1199–1210, https://doi.org/10.1016/S1352-2310(02)01017-8, 2003.

Schade, J., Passig, J., Irsig, R., Ehlert, S., Sklorz, M., Adam, T., Li, C., Rudich, Y., and Zimmermann, R.: Spatially Shaped Laser Pulses for the Simultaneous Detection of Polycyclic Aromatic Hydrocarbons as well as Positive and Negative Inorganic Ions in Single Particle Mass Spectrometry, Anal. Chem., 91, 10282–10288, https://doi.org/10.1021/acs.analchem.9b02477, 2019.

Seinfeld, J. H. and Pandis, S. N.: Atmospheric Chemistry and Physics: From Air Pollution to Climate Change, 3rd ed., Wiley, s.l., 2185 pp., 2016.

Seyler, A., Wittrock, F., Kattner, L., Mathieu-Üffing, B., Peters, E., Richter, A., Schmolke, S., and Burrows, J. P.: Monitoring shipping emissions in the German Bight using MAX-DOAS measurements, Atmos. Chem. Phys., 17, 10997–11023, https://doi.org/10.5194/acp-17-10997-2017, 2017.

Shields, L. G., Suess, D. T., and Prather, K. A.: Determination of single particle mass spectral signatures from heavy-duty diesel vehicle emissions for PM2.5 source apportionment, Atmospheric Environ., 41, 3841–3852, https://doi.org/10.1016/j.atmosenv.2007.01.025, 2007.

Sippula, O., Stengel, B., Sklorz, M., Streibel, T., Rabe, R., Orasche, J., Lintelmann, J., Michalke, B., Abbaszade, G., Radischat, C., Gröger, T., Schnelle-Kreis, J., Harndorf, H., and Zimmermann, R.: Particle emissions from a marine engine: chemical composition and aromatic emission profiles under various operating conditions, Environ. Sci. Technol., 48, 11721–11729, https://doi.org/10.1021/es502484z, 2014.

Sofiev, M., Winebrake, J. J., Johansson, L., Carr, E. W., Prank, M., Soares, J., Vira, J., Kouznetsov, R., Jalkanen, J.-P., and Corbett, J. J.: Cleaner fuels for ships provide public health benefits with climate tradeoffs, Nat. Commun., 9, 406, https://doi.org/10.1038/s41467-017-02774-9, 2018.

Song, X.-H., Hopke, P. K., Fergenson, D. P., and Prather, K. A.: Classification of Single Particles Analyzed by ATOFMS Using an Artificial Neural Network, ART-2A, Anal. Chem., 71, 860–865, https://doi.org/10.1021/ac9809682, 1999.

Spencer, M. T., Shields, L. G., Sodeman, D. A., Toner, S. M., and Prather, K. A.: Comparison of oil and fuel particle chemical signatures with particle emissions from heavy and light duty vehicles, Atmos. Environ., 40, 5224–5235, https://doi.org/10.1016/j.atmosenv.2006.04.011, 2006.

Stein, A. F., Draxler, R. R., Rolph, G. D., Stunder, B. J. B., Cohen, M. D., and Ngan, F.: NOAA's HYSPLIT Atmospheric Transport and Dispersion Modeling System, Bull. Am. Meteorol. Soc., 96, 2059–2077, https://doi.org/10.1175/BAMS-D-14-00110.1, 2015.

Streibel, T., Schnelle-Kreis, J., Czech, H., Harndorf, H., Jakobi, G., Jokiniemi, J., Karg, E., Lintelmann, J., Matuschek, G., Michalke, B., Müller, L., Orasche, J., Passig, J., Radischat, C., Rabe, R., Reda, A., Rüger, C., Schwemer, T., Sippula, O., Stengel, B., Sklorz, M., Torvela, T., Weggler, B., and Zimmermann, R.: Aerosol emissions of a ship diesel engine operated with diesel fuel or heavy fuel oil, Environ. Sci. Pollut. Res. Int., 24, 10976–10991, https://doi.org/10.1007/s11356-016-6724-z, 2017.

Sultana, C. M., Cornwell, G. C., Rodriguez, P., and Prather, K. A.: FATES: a flexible analysis toolkit for the exploration of single-particle mass spectrometer data, Atmos. Meas. Tech., 10, 1323–1334, https://doi.org/10.5194/amt-10-1323-2017, 2017.

Tian, J., Riemer, N., West, M., Pfaffenberger, L., Schlager, H., and Petzold, A.: Modeling the evolution of aerosol particles in a ship plume using PartMC-MOSAIC, Atmos. Chem. Phys., 14, 5327–5347, https://doi.org/10.5194/acp-14-5327-2014, 2014.

Toner, S. M., Shields, L. G., Sodeman, D. A., and Prather, K. A.: Using mass spectral source signatures to apportion exhaust particles from gasoline and diesel powered vehicles in a freeway study using UF-ATOFMS, Atmospheric Environment, 42, 568–581, https://doi.org/10.1016/j.atmosenv.2007.08.005, 2008.

Toner, S. M., Sodeman, D. A., and Prather, K. A.: Single Particle Characterization of Ultrafine and Accumulation Mode Particles from Heavy Duty Diesel Vehicles Using Aerosol Time-of-Flight Mass Spectrometry, Environ. Sci. Technol., 40, 3912–3921, https://doi.org/10.1021/es051455x, 2006.

Van Roy, W and Scheldemann, K.: Results MARPOL Annex VI Monitoring Report Belgian Sniffer campaign 2016, CompMon, https://arkisto.trafi.fi/filebank/a/1482762219/4ba0baf93df900f6ac151919f527e2bc/23540-Results_Belgian_Sniffer_Campagin_2016-consealed.pdf, last access: 23 November 2020, 2016.

Viana, M., Hammingh, P., Colette, A., Querol, X., Degraeuwe, B., Vlieger, I. de, and van Aardenne, J.: Impact of maritime transport emissions on coastal air quality in Europe, Atmospheric Environ., 90, 96–105, https://doi.org/10.1016/j.atmosenv.2014.03.046, 2014.

Viana, M., Amato, F., Alastuey, A., Querol, X., Moreno, T., García Dos Santos, S., Herce, M. D., and Fernández-Patier, R.: Chemical Tracers of Particulate Emissions from Commercial Shipping, Environ. Sci. Technol., 43, 7472–7477, https://doi.org/10.1021/es901558t, 2009.

Wang, X., Shen, Y., Lin, Y., Pan, J., Zhang, Y., Louie, P. K. K., Li, M., and Fu, Q.: Atmospheric pollution from ships and its impact on local air quality at a port site in Shanghai, Atmos. Chem. Phys., 19, 6315–6330, https://doi.org/10.5194/acp-19-6315-2019, 2019.

Winebrake, J. J., Corbett, J. J., Green, E. H., Lauer, A., and Eyring, V.: Mitigating the Health Impacts of Pollution from Oceangoing Shipping: An Assessment of Low-Sulfur Fuel Mandates, Environ. Sci. Technol., 43, 4776–4782, https://doi.org/10.1021/es803224q, 2009.

Winnes, H., Granberg, M., Magnusson, K., Malmaeus, K., Mellin, A., Stripple, H., Yaramenka, K., and Zhang, Y.: Scrubbers: Closing the loop; Activity 3. Summary, IVL Swedish Environmental Research Institute, https://www.ivl.se/publikationer/publikation.html?id=5737, last access: 30 November 2020, 2018.

Winnes, H., Fridell, E., and Moldanová, J.: Effects of Marine Exhaust Gas Scrubbers on Gas and Particle Emissions, J. Mar. Sci. Eng., 8, 2020.

Xiao, Q., Li, M., Liu, H., Fu, M., Deng, F., Lv, Z., Man, H., Jin, X., Liu, S., and He, K.: Characteristics of marine shipping emissions at berth: profiles for particulate matter and volatile organic compounds, Atmos. Chem. Phys., 18, 9527–9545, https://doi.org/10.5194/acp-18-9527-2018, 2018.

Ye, D., Klein, M., Mulholland, J. A., Russell, A. G., Weber, R., Edgerton, E. S., Chang, H. H., Sarnat, J. A., Tolbert, P. E., and Ebelt Sarnat, S.: Estimating Acute Cardiovascular Effects of Ambient PM2.5 Metals, Environ. Health Perspect., 126, 27007, https://doi.org/10.1289/EHP2182, 2018.

Yu, C., Pasternak, D., Lee, J., Yang, M., Bell, T., Bower, K., Wu, H., Liu, D., Reed, C., Bauguitte, S., Cliff, S., Trembath, J., Coe, H., and Allan, J. D.: Characterizing the Particle Composition and Cloud Condensation Nuclei from Shipping Emission in Western Europe, Environ. Sci. Technol., https://doi.org/10.1021/acs.est.0c04039, 2020.

Zhang, F., Chen, Y., Tian, C., Wang, X., Huang, G., Fang, Y., and Zong, Z.: Identification and quantification of shipping emissions in Bohai Rim, China, The Science of the total environment, 497-498, 570–577, https://doi.org/10.1016/j.scitotenv.2014.08.016, 2014.

Zhang, Y., Deng, F., Man, H., Fu, M., Lv, Z., Xiao, Q., Jin, X., Liu, S., He, K., and Liu, H.: Compliance and port air quality features with respect to ship fuel switching regulation: a field observation campaign, SEISO-Bohai, Atmos. Chem. Phys., 19, 4899–4916, https://doi.org/10.5194/acp-19-4899-2019, 2019.

Zhou, F., Hou, L., Zhong, R., Chen, W., Ni, X., Pan, S., Zhao, M., and An, B.: Monitoring the compliance of sailing ships with fuel sulfur content regulations using unmanned aerial vehicle (UAV) measurements of ship emissions in open water, Atmos. Meas. Tech., 13, 4899–4909, https://doi.org/10.5194/amt-13-4899-2020, 2020.

Zhou, Y., Huang, X. H., Griffith, S. M., Li, M., Li, L., Zhou, Z., Wu, C., Meng, J., Chan, C. K., Louie, P. K., and Yu, J. Z.: A field measurement based scaling approach for quantification of major ions, organic carbon, and elemental carbon using a single particle aerosol mass spectrometer, Atmos. Environ., 143, 300–312, https://doi.org/10.1016/j.atmosenv.2016.08.054, 2016.

Zimmermann, Ralf and Hanley, Luke (Ed.): Laser Ionization in Single-Particle Mass Spectrometry.

Seite 15: [1] Formatiert	Johannes Passig	19.03.2021 18:43:00

Schriftart: (Standard) +Textkörper (Times New Roman)

Seite 15: [2] Formatiert	Johannes Passig	19.03.2021 18:43:00

Schriftart: (Standard) +Textkörper (Times New Roman)

Seite 15: [3] Formatiert	Johannes Passig	19.03.2021 18:43:00

Schriftart: (Standard) +Textkörper (Times New Roman)

Seite 15: [4] Formatiert	Johannes Passig	19.03.2021 18:43:00

Schriftart: (Standard) +Textkörper (Times New Roman)

Seite 15: [5] Formatiert	Johannes Passig	19.03.2021 18:43:00

Schriftart: (Standard) +Textkörper (Times New Roman)

Seite 15: [6] Formatiert	Johannes Passig	19.03.2021 18:43:00

Schriftart: (Standard) +Textkörper (Times New Roman)

Seite 15: [7] Formatiert	Johannes Passig	19.03.2021 18:43:00

Schriftart: (Standard) +Textkörper (Times New Roman)

Seite 15: [8] Formatiert	Johannes Passig	19.03.2021 18:43:00

Schriftart: (Standard) +Textkörper (Times New Roman)

Seite 15: [9] Formatiert	Johannes Passig	19.03.2021 18:43:00

Schriftart: (Standard) +Textkörper (Times New Roman)

Seite 15: [10] Formatiert	Johannes Passig	19.03.2021 18:43:00

Schriftart: (Standard) +Textkörper (Times New Roman)

Seite 15: [11] Formatiert	Johannes Passig	23.03.2021 10:45:00

Schriftart: (Standard) +Textkörper (Times New Roman)

Seite 15: [12] Formatiert	Johannes Passig	23.03.2021 10:45:00

Schriftart: (Standard) +Textkörper (Times New Roman)

Seite 15: [13] Formatiert	Johannes Passig	23.03.2021 10:45:00

Schriftart: (Standard) +Textkörper (Times New Roman)

Seite 15: [14] Formatiert	Johannes Passig	23.03.2021 10:45:00

Schriftart: (Standard) +Textkörper (Times New Roman)

Seite 15: [15] Formatiert	Johannes Passig	23.03.2021 10:45:00

Schriftart: (Standard) +Textkörper (Times New Roman)

Seite 15: [16] Formatiert	Johannes Passig	23.03.2021 10:45:00

Schriftart: (Standard) +Textkörper (Times New Roman)

Seite 15: [17] Formatiert	Johannes Passig	23.03.2021 10:45:00

Schriftart: (Standard) +Textkörper (Times New Roman)

Seite 15: [18] Formatiert	Johannes Passig	23.03.2021 10:45:00

Schriftart: (Standard) +Textkörper (Times New Roman)